European Journal of Medicinal Chemistry 207 (2020) 112797

Contents lists available at ScienceDirect

European Journal of Medicinal Chemistry

journal homepage: http://www.elsevier.com/locate/ejmech

Research paper

Synthesis, biological evaluation, in silico modeling and crystallization of novel small monocationic molecules with potent antiproliferative activity by dual mechanism

Lucía Serrán- Aguilera [a, 1], Elena Mariotto [b, 1], Gianluca Rubbini [a], Francisco Fermín Castro Navas [a], Carmen Marco [c], María Paz Carrasco-Jiménez [c], Marco Ballarotto [d], Antonio Macchiarulo [d], Ramón Hurtado-Guerrero [e, f], Giampietro Viola [b], Luisa Carlota Lopez-Cara [a, *]

[a] Department of Pharmaceutical and Organic Chemistry, Faculty of Pharmacy, Campus Cartuja S/n. University of Granada, 18010, Granada, Spain
[b] Department of Woman's and Child's Health, Laboratory of Oncohematology, University of Padova, 35128, Padova, Italy
[c] Department of Biochemistry and Molecular Biology I, Faculty of Sciences, 18071, Granada, Spain
[d] Department of Pharmaceutical Sciences, University of Perugia, Via Del Liceo 1, Perugia, 06123, Italy
[e] Institute of Biocomputation and Physics of Complex Systems (BIFI), University of Zaragoza, Institute for Biocomputation and Physics of Complex Systems (BIFI) and Laboratorio de Microscopías Avanzada (LMA), Mariano Esquillor S/n, Campus Rio Ebro, Edificio I+D; Fundacion ARAID, 50018, Zaragoza, Spain
[f] Copenhagen Center for Glycomics, Department of Cellular and Molecular Medicine, School of Dentistry, University of Copenhagen, Copenhagen, Denmark

ARTICLE INFO

Article history:
Received 5 May 2020
Received in revised form
28 August 2020
Accepted 30 August 2020
Available online 6 September 2020

Keywords:
Antitumoral drug
Choline kinase inhibition
Choline uptake

ABSTRACT

Seeking for new anticancer drugs with strong antiproliferative activity and simple molecular structure, we designed a novel series of compounds based on our previous reported pharmacophore model composed of five moieties. Antiproliferative assays on four tumoral cell lines and evaluation of Human Choline Kinase CKα1 enzymatic activity was performed for these compounds. Among tested molecules, those ones with biphenyl spacer showed betters enzymatic and antiproliferative activities (**n-v**). Docking and crystallization studies validate the hypothesis and confirm the results. The most active compound (**t**) induces a significant arrest of the cell cycle in G0/G1 phase that ultimately lead to apoptosis, following the mitochondrial pathway, as demonstrated for other choline kinase inhibitors. However additional assays reveal that the inhibition of choline uptake could also be involved in the antiproliferative outcome of this class of compounds.

1. Introduction

Cancer is among the main world causes of mortality and morbidity, further exacerbated by the occurrence of drug resistance [1]. For this reason, despite being an intensively investigated disease, new drugs and therapeutic strategies are still urgently needed to more efficiently eradicate cancer cells. their transcriptional and mutational heterogeneity, cancer cells derived from different types of tumors frequently share similar metabolic abnormalities, such as changes in energy metabolism, from oxidative phosphorylation to aerobic glycolysis, increased protein and nucleotide synthesis and increased lipogenesis, in order to satisfy the demand in the synthesis of biomolecules that proliferation requires [2,3]. Among the lipid-related alterations, it has been described that many types of cancer show an abnormal metabolism of phospholipids containing choline and/or ethanolamine [4,5], which can be a starting point in the design of new antitumor strategies.

The involvement of choline (Cho) metabolism and cancer has been demonstrated by magnetic resonance spectroscopy images, which highlight the presence of the "choline phenotype" in multiple tumors, characterized by high levels of phosphocholine and in general of choline-containing compounds [4].

Phosphatidylcholine (PC) is not only the most abundant phospholipid in cell membranes but also constitutes a fundamental part of lipoproteins, biliary lipids and lung surfactants [6,7], besides being a direct substrate for the synthesis of sphingomyelins (SM) and an essential source of second messengers. PC can be

* Corresponding author.
E-mail address: lcarlotalopez@ugr.es (L.C. Lopez-Cara).
[1] Equal contributing Authors.

https://doi.org/10.1016/j.ejmech.2020.112797
0223-5234/

synthesized from choline, an organic cation that cannot cross plasma membrane freely, needing therefore active transporters to enter into the cell [8,9]. Once choline is inside the cell, it can follow several pathways becoming incorporated to diverse cellular components. One of these is the **Kennedy pathway** or CDP-choline pathway, which leads to the synthesis of PC. This pathway consists of three steps catalysed by different enzymes. The first step of PC synthesis is catalysed by the cytosolic enzyme choline kinase (**CK**) which drive the ATP-dependent phosphorylation of choline in the presence of magnesium [10]. The human choline kinases family comprises three isoforms, **CKα1** (457 residues, 52 kDa), **CKα2** (439 residues, 50 kDa) that both originate from *chok-α* gene, and **CKβ** (395 residues, 45 kDa) encoded by *chok-β* gene. Elevated expression of CKα has been reported for many tumors where it correlates with an unfavourable prognosis [11,12], thus becoming a new tumor metabolic marker involved in the "choline phenotype".

Recently our group has shown that in HepG2 cells the **EB-3D CKα1** inhibitor [13–16] interferes with PC biosynthesis through 1) the choline uptake and 2) the CDP-choline synthesis pathway. This effect is accompanied by a significant decrease in cholesterol biosynthesis, as well as alterations in the expression of proteins related to lipid homeostasis. We also found that, surprisingly, **EB-3D** reduces **CKα** protein levels. All these alterations could be explained by the modulation of the AMPK signalling pathway [16]. Our results conclude that **EB-3D** has an antitumor activity underlying a deregulation of lipid metabolism [14]. As mentioned above, it is possible that some of the CK inhibitors could inhibit not only the enzyme but also choline uptake in accordance with some authors which reported the dual behaviour of certain choline kinase inhibitors [28,29].

The deconvolution studies in monocationic asymmetrical compounds determined that the adenine fragment occupies the ATP binding site and that the pyridinium fragment, though its positive charge is delocalized over the aromatic ring, mimics the positive charge present in choline [17,18]. This situation was similar for biscationic asymmetrical compounds with biphenyl group as a linker [19]. However, the biscationic asymmetrical compounds with a linker of 4 carbon atoms showed an unprecedented binding mode to CKα1 [19]. On the other hand, recent docking studies have showed that the same behaviour occurs in asymmetrical biscationic compounds with a pyridinium and quinolinium cationic heads [13,20,21].

Moreover, we recently proposed a pharmacophore model composed of five moieties (RRRPN: the positive charge of the pyridinium ring - feature P; a nitrogen atom - feature N; and three aromatic groups - features R) that are included in the 1-benzyl-4-(*N*-methylaniline) pyridinium fragment [22,23]. The comparison with compounds with a phenyl ring condensed to the pyridine (quinolinium derivatives) has showed that the extended conjugation is not essential for the enzyme inhibition [22,23]. At the same time, Zech et al. [24] through another computational study described a pharmacophore model consisting of small molecules without the second positive charge, with tertiary amines (diazepanes or piperazines) that present a better safety profile. In addition, a dose-dependent correlation between the enzymatic inhibition, the antiproliferative effect and apoptosis has been observed for these molecules [24].

These results prompted us to synthesise and evaluate a series of small monocationic molecules wherein our pharmacophore is included, but also other ones wherein this pharmacophore has been modified with other moieties, in order to establish a structure-activity relationship (SAR) and refine the pharmacophoric hypothesis. Hence, we design and synthesized firstly a series of compounds with phenyl pyridinium and (7-chloro)-quinolinium moieties *N*-substituted in 4 position with cycloalkylamines or with *N*,*N*-methylphenyl fragment. In order to set a SAR electron withdrawing group trifluoromethyl, (-CF_3) and a phenyl ring have been introduced, obtaining the second and third series of compounds (A, B and C) as a substituent $\mathbf{R_3}$.

The cationic heads of the three series have been chosen based on the pharmacophore and the chemical structure-activity relations previously established by our research group [13,20,21,25]. In particular, the cationic heads of the series A, B and C were chosen on the basis that: a) they allow us to study whether the phenyl group attached to the exocyclic nitrogen of the pharmacophore can be dispensed with and whether the fusion of a phenyl ring to the pyridine ring optimizes the pharmacophore; b) they have demonstrated their suitability for the design of CK inhibitors over the last few years. Consequently, functional groups derived from pyridine (dimethylamino- and pyrrolidinopyridine) and quinolines (phenyl- or cycloalkylaminoquinoline) and quinuclidine were selected for this study.

The purpose of this study is twofold. On one hand, the aim is to optimise the pharmacophore by studying whether any of the five functional groups that define it is dispensable, for which the fragment of 1-benzyl-4-(*N*-methylanilino)pyridinium will be pharmacomodulated. On the other hand, the aim is to achieve a greater degree of affinity for human CKα1 and, consequently, a better inhibitory and antiproliferative power than that shown by the prototypes from virtual screening [22].

Within the **A** and **B** (Chart 1) series we distinguish thirteen compounds benzyl and *p*-trifluoromethylbenzyl derivatives depending on whether the cationic head is derived from pyridine (4-(*N*,*N*-dimethylamino)pyridine, 4-pyrrolidinopyridine), quinoline (7-chloro-4-(*N*-methylanilino)quinoline, 7-chloro-4-(perhydroazepin-1-yl)quinoline), 7-chloro-4-(*N*-methylaniline) quinoline) or quinuclidine.

The **A** and **B** series (Chart 1) aim to clarify whether these simple structures show affinity for the enzyme as pointed out by the pharmacophore or whether, on the contrary, they require the introduction of more functional groups to improve their binding. Another objective will be to determine the affinity differences between pyridine and quinoline derivatives, both on the basis of the phenyl ring fused with pyridine and on the basis of the exocyclic amino substituents in position 4.

In the **C** series (Chart 1) the structures were optimized by introducing one more phenyl group into the spacer, with the purpose of increasing the enzyme affinity through π-π interactions with the aromatic residues present at the choline site. This small modification will allow a comparison of the affinity, inhibitory activity and antiproliferative capacity of these derivatives with those of the **A** and **B** series.

2. Chemistry

These compounds **a-v** have been synthesized using microwaves in one easy step. To a prepared solution of benzyl bromide, 1-(bromomethyl)-4-(trifluoromethyl)benzene or 4-(bromomethyl)-1,1′-biphenyl in butanone or acetonitrile as the solvent, was added the corresponding intermediates **1**–**3**, (7-chloro)-4-subtituted quinoline **4,** quinuclidine **5**, or 3-quinuclidinol **6** [13,20,21,25] (in a molar ratio of 1:1). The reaction was performed in a sealed tube a under microwave irradiation (140 °C, 28–33 min). (Scheme 1).

3. Biological results and discussion

3.1. In vitro antiproliferative activities

Table 1 summarizes the growth inhibitory effects of derivatives **a**–**v** and reference compounds **RSM932A** and **MN58b** (Chart 1)

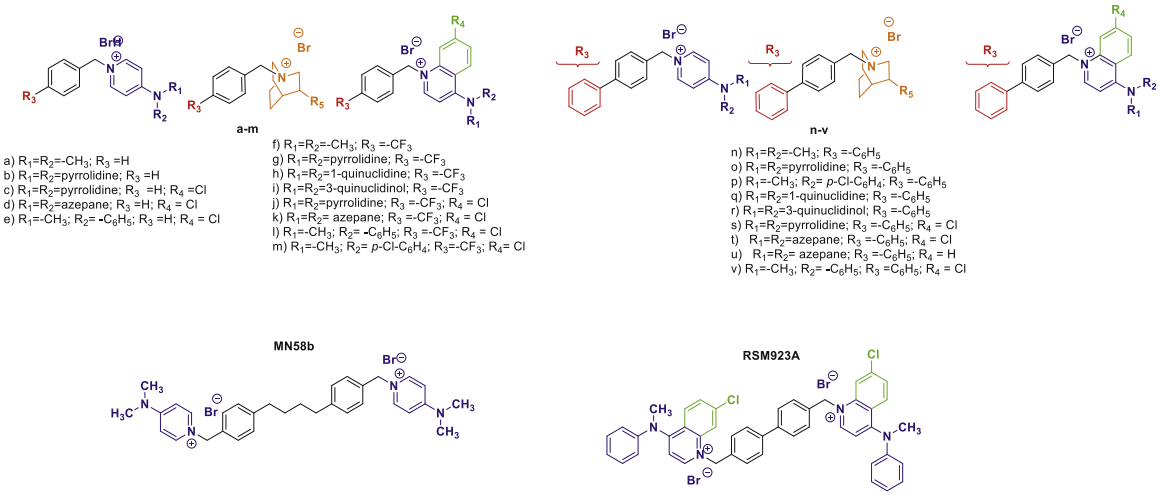

Chart 1. General structure of **series A, B** and **C** (**a-v**). Reference compounds **MN58b** and **RSM932A**.

against a panel of four human cancer cell lines. The results presented in Table 1 indicate that inhibition of cell growth was highly dependent upon the presence of a second phenyl ring as R_3 substituent, being the most active compounds belonging to series C. The first remark is that the quinuclidinium moiety (**h**, **i**, **q** and **r**) drastically decrease the activity, which is in agreement with our previous results [13,20,21,25].

Moreover, we can also observe that the less active compounds are those bearing a phenyl ring without substituent. The presence of substituent groups in position 4 (R_3), such as trifluoromethyl (-CF_3) or a second phenyl group, significantly increases the antiproliferative activity, with this increment being higher for the C series. Hence, the enhancement of potency seems to be related to the increase in lipophilicity/volume of the compounds (see the values of clogP in Table 1), that can better fit into the markedly hydrophobic enzyme pocket.

Compounds with quinolinic rings (**c-e**, **j-m** and **s-v**) lead to lower values of GI_{50} (μM) with respect to pyridinium derivatives (**a-b**, **f-g** and **n-p**). Moreover, the worse results are obtained when the substituent in 4 position is a *N*-methylaniline. (**s-t** *vs* **v**). Finally, the presence of a chlorine atom in position 7 of quinolinium moiety greatly increases the activity up to 200-fold (in RS4; 11 **t** *vs* **u**). However, this effect is negligible when the chlorine atom is found in *para* position of the *N*-methylaniline fragment (**l** *vs* **m**), indicating a non-proper accommodation of the compounds over the enzymatic pocket of *CKα1.*

3.2. *Affinity and selectivity of compounds **a-v** for CKα1*

The evaluation of the affinity of monocationic derivatives for the different isoforms of CK (CKα1 and CKβ) was carried out by fluorescence spectroscopy. This technique is very useful due to the presence of tryptophan residues at the choline binding site. All compounds were tested with CKα1 and some also with CKβ to study their selectivity.

The selected compounds belong to the **A** (**a**, **b**, **d**, and **e**) and to the **C** series (**n**, **o**, **t** and **v**). In addition, in order to evaluate the effect of the positive charge and benzyl group of the different compounds on protein affinity, control experiments were performed with non-quaternized forms of the cationic heads. That is, 4-dimethylaminopyridine (DMAP), 4-pyrrolidinopyridine (PPIR), 7-chloro-4-(perhydroazepin-1-yl)quinoline (QUINAZE) and 7-chloro-4-(*N*-methylanilino)quinoline (QUINPHEN) (Fig. 1).As depicted in Table 2, the four reference compounds showed very little affinity (35–82 μM) for CK thus demonstrating the importance of the positive charge to achieve efficient ligand binding. However, although their effect is not very noticeable, some affinity for the enzyme is still shown thanks to the aromatic rings. In general, the least related compounds were those of the **A** series (K_d between 0.4 and 24 μM, Table 2) while the compounds from the **C** family were recognized by the protein with a very similar affinity (0.185–1.7 μM, Table 2). A remarkable improvement in affinity is also observed in quinoline derivatives over pyridinium for all classes, suggesting that some type of favorable interaction with the protein must be established by the quinoline rings. Consequently, it can be said that the compounds bind to CKα1 with an increasing affinity as the complexity of their chemical structure increases, which could be related to the type and number of interactions they are able to establish with the residues of the active site.

For Series **A,** the quaternization by a benzyl group of the endocyclic nitrogen noticeably increases the affinity with the protein, in accordance with the pharmacophore model. Also, the

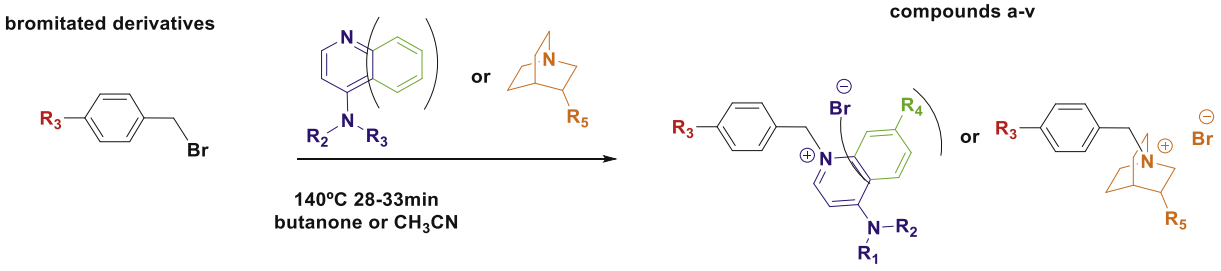

Scheme 1. General synthetic pathway for final compounds **a-v.**

Table 1
In vitro inhibitory effects of compounds a-v.

Series	Comp.	clogP[b]	GI_{50} (μM)[a]			
			HeLa	HT-29	RS4; 11	CCRF-CEM
A	**a**	−0.0630	44.2 ± 0.4	>100	30.3 ± 2.3	54.3 ± 0.9
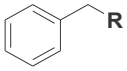	**b**	0.0509	66.0 ± 0.6	38.0 ± 0.6	8.3 ± 3.0	5.3 ± 0.8
	c	2.19	19.6 ± 0.8	4.1 ± 0.16	1.23 ± 0.06	3.4 ± 1.3
	d	3.31	16.2 ± 1.1	4.6 ± 0.14	0.03 ± 0.008	0.56 ± 0.11
	e	3.84	16.3 ± 4.6	4.5 ± 0.16	3.0 ± 0.6	2.2 ± 0.06
B	**f**	0.82	23.2 ± 0.9	11.2 ± 0.37	7.9 ± 0.9	18.0 ± 2.4
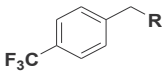	**g**	0.934	42.1 ± 1.9	8.1 ± 0.22	7.6 ± 0.26	12.0 ± 2.6
	h	0.353	90.8 ± 2.1	>100	>100	>100
	i	0.103	82.3 ± 4.4	>100	>100	>100
	j	3.07	15.0 ± 0.6	12.9 ± 0.37	1.0 ± 0.28	3.0 ± 1.1
	k	4.19	4.7 ± 0.37	5.4 ± 1.4	3.2 ± 0.5	4.6 ± 0.37
	l	4.73	2.1 ± 0.2	3.0 ± 0.12	2.7 ± 0.3	2.1 ± 0.16
	m	5.47	2.6 ± 0.09	1.3 ± 0.12	1.3 ± 0.03	2.0 ± 0.05
C	**n**	1.82	0.74 ± 0.02	0.29 ± 0.01	0.83 ± 0.14	0.43 ± 0.03
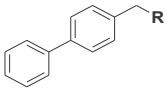	**o**	1.93	0.95 ± 0.41	0.16 ± 0.07	0.22 ± 0.03	0.18 ± 0.10
	p	4.36	0.91 ± 0.12	0.23 ± 0.03	0.14 ± 0.02	0.30 ± 0.05
	q	1.35	29.9 ± 4.9	24.7 ± 2.3	2.6 ± 0.75	11.8 ± 3.5
	r	1.10	27.5 ± 2.9	34.0 ± 1.5	1.7 ± 0.8	16.9 ± 3.5
	s	4.08	0.28 ± 0.07	0.04 ± 0.003	0.05 ± 0.006	0.04 ± 0.01
	t	4.44	0.36 ± 0.05	0.09 ± 0.009	0.06 ± 0.002	0.15 ± 0.06
	u	5.19	14.8 ± 1.8	17.5 ± 0.30	12.8 ± 4.5	8.6 ± 1.8
	v	5.73	1.7 ± 0.06	0.85 ± 0.12	1.4 ± 0.17	1.7 ± 0.06
RSM932A[c]			0.83 ± 0.1	0.4 ± 0.2	0.17 ± 0.04	0.61 ± 0.20
MN58b[c]			1.9 ± 0.1	1.9 ± 0.4	1.0 ± 0.3	0.21 ± 0.09

[a] GI^{50} = compound concentration required to inhibit tumor cell proliferation by 50%. Values are the mean ± SE from the dose-response curves of at least three independent experiments carried out in triplicate.
[b] The values of clogP were calculated with Chemdraw 15.0.
[c] Data taken from ref. 36 *Scientific Reports*. **2016**, *6*, 2379.

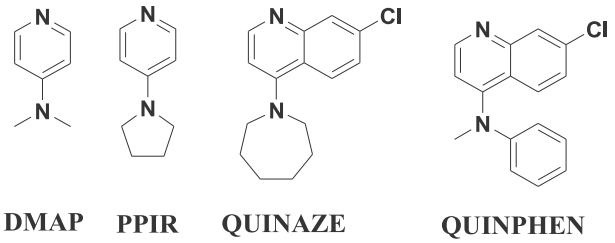

Fig. 1. Unquaternized control ligands.

increment in lipophilicity of compounds **d** and **e** (clog P Table 1) supports the influence of this molecular property on the binding affinity. Lastly, the slightly greater affinity shown by compound **d** with respect to **e** suggests that the phenyl ring of the *N*-methylaniline group of the pharmacophoric hypothesis is not essential to achieve an efficient binding to the protein.

The affinity for CKα1 of the compounds of the series **C** is greater than that of the compounds of the previous series. Noticeably, the improvement in affinity in relation to their analogues of the series **A** is greater in the K_d pyridine derivatives (**n** and **o**), than the quinoline derivatives (**t** and **v**). Again, it is observed that quinoline derivatives bind better to the protein than pyridines and specifically, the compound with 7-chloro-4-(*N*-methylanilino)quinoline (**v**) shows a greater affinity than **t**.

Consequently, it can be inferred that the affinity of **A**-series compounds for CK can be improved by introducing an additional phenyl group into the spacer, as observed for the final **C**-series compounds. In addition, the similarity of affinities between compounds with and without the *N*-methylaniline phenyl group demonstrates once again that it is not essential to achieve protein binding. However, if present, it improves the binding affinity, as does the additional phenyl of the quinolinium ring.

All these data can be translated into the fact that probably of all

Table 2
Tryptophan fluorescence spectroscopy choline kinase data. Selected compounds for fluorescence assays and K_d values versus CKα1 and CKβ.

	DMAP	PPIR	QUINAZE	QUINPHEN
K_d (μM)[a] CKα1	35 ± 18	49 ± 3	45 ± 3	82 ± 12
Series A	**a**	**b**	**d**	**e**
K_d (μM) CKα1	14 ± 0,7	24 ± 3.5	0.40 ± 0.04	0.89 ± 0,047
K_d (μM)[b] CKβ	–	–	33 ± 5 (83)[c]	36 ± 5 (41)[c]
Series C	**n**	**O**	**t**	**v**
K_d (μM) CKα1	1.7 ± 0.045	0.67 ± 0,002	0.37 ± 0.80	0.185 ± 0.024
K_d (μM) CKβ	–	–	63 ± 3 (171)[c]	20 ± 5 (108)[c]

[a,b] K_ds values of indicated compounds for CKα1 or CKβ are represented as mean ± S.D. of at least three independent experiments.
[c] Fold increase respect to CKα1.

the chemical fragments present in the pharmacophore (three aromatic rings: benzyl, pyridine and *N*-methylaniline, positive charge and exocyclic nitrogen), the most important to achieve an efficient binding to CK are the delocalized positive charge in the heteroaromatic ring, the benzyl group attached to the charged atom and the exocyclic nitrogen. The remaining functional group, i.e. benzene from the *N*-methylaniline group does not appear to be indispensable, but if present, in some cases (compound **v**) it may contribute slightly to improving the affinity of the compounds.

On the other hand, as it has recently been shown that a potent anticarcinogenic effect can only be achieved when the expression of CKα1 is specifically decreased without affecting the levels of CKβ [26]. So, the selective binding of some of these new synthetic derivatives to the isoform CKα1 was evaluated. For this, fluorescence experiments were carried out against the isoform CKβ. According to the K_d values obtained, these compounds are selective for CKα1, with compound **t** showing the highest selectivity (Table 2). The selective character of the ligands is attributed to the greater

flexibility of Trp420 at CKα1 compared to that of its counterpart (Trp353) at CKβ, since in the isoform α1 there is a leucine behind tryptophan, instead of the phenylalanine of the isoform β. For this reason, the selectivity of the compounds could be linked to their binding mode to the CK, more specifically to shift of the tryptophan residue needed to host the ligand at the site of the choline. Thus, in view of the selectivity data it could be hypothesized that to host the compound **t**, it might be necessary for the shift of Trp420 to increase the size of the cavity (given the volume of the compound) or to interact with some functional group of the ligand. In the case of the isoform α such displacement would be possible, while in the case of the isoform CKβ, it would be prevented by the bulkier phenylalanine.

3.3. Inhibition of human CKα1

Taking into account the second catalytic mechanism proposed for CK [27], this implies that potential inhibitors that have been designed to act at the level of the choline site must hinder the nucleophilic attack of Asp306 on the phosphate γ of the ATP or, if this occurs, to be effective, they should not be displaced from the active site after phosphorylation of that residue. By inspecting the properties of the choline binding site, adequate ligand affinity is achieved with interactions engaging aromatic residues of this hydrophobic pocket. Accordingly, functional groups amenable to such interactions should be brought together in a single ligand according to the geometrical features reported in the pharmacophore model, including a positive charge, three aromatic rings and an exocyclic nitrogen [22].

The results of the effect of tested compounds on the CKα1 activity are shown in Table 3. In general, it can be observed that the effects on the inhibition are better for the more voluminous the ligand, i.e. starting from series **A** to series **B** and then to series **C**. The highest inhibition values were obtained for compounds **t** and **v** (94% and 76% to 30 μM respectively), in good agreement with their cytotoxic potency (Table 1). Considered that both compounds presented a low value of K_d, these results confirm that the greater the affinity of the ligand for the protein, the greater the inhibitory action on CKα1.

Albeit the series **A** compounds bind to the choline site with an affinity of 0.4–24 μM (Table 2), no significant differences are observed between the **A** and **B** series, indicating that the introduction of the trifluoromethyl group as an electron-withdrawing group has a poor effect on enzyme inhibition. In this case, the increase in inhibition in quinoline derivatives is not too evident, so that compound **a** inhibits in higher values to compound **e**. While for compounds **b** and **d** occurs the opposite, where there is an 11% at 50 μM, increase in inhibitory activity for compound **d** (38%) in relation to **b** (28%) (Table 3).

In the case of compounds of series **C**, fluorescence indicated that the introduction of an additional phenyl in the spacer led to an increase in enzyme affinity with respect to series **A** derivatives. According to inhibition data (Table 3), this observation is confirmed for quinoline derivatives. Specifically, compound **t** has a IC_{50} of 6.74 μM, while the IC_{50} of the compound **v** is 12.55 μM. It is worth to note that compounds with quinuclidinium moiety as cationic head (**h-i** and **q-r**) moderately inhibit the enzyme and have weak antiproliferative effects, that can be likely ascribed to the low lipophilicity of these derivatives (Table 1).

3.4. Crystallographic studies

Crystallographic studies with at least one representative from each family (**b** and **o** compounds) were conducted to have experimental evidence in this regard and to explain the gradual increase in affinity and inhibitory potency.

The crystalline structures of CKα1 in complex with each of the compounds (Fig. 2) were obtained with a resolution between 1,55-2,30 Å (Table 4) and good statistic parameters (R = 0,189–0,201, R_{free} = 0,214–0,257, Table 4) after an iterative process of construction and refining.

Both crystalline structures are homodimeric, each monomer is made up of a small *N*-terminal domain and a larger C-terminal domain. While the ATP binding site is located in a cleft formed by the residues of both *N*- and *C*-terminal domains, the choline site is in a deep, hydrophobic pocket of the *C*-terminal domain. Surprisingly, presence of two molecules of compound **o** at the choline binding site was observed (Fig. 2b). Conversely, only one molecule of compound **b** was observed (Fig. 2a). This is probably due to the fact that the positioning of its ligands in this common site is more favorable from an energetic point of view, and only occasionally does it obtain enough energy to introduce the ligands in the second site.

The compounds belonging to the **A** and **B** series were those that showed a weaker affinity and inhibitory activity. According to the evidence provided by the crystal of the complex CKα1/**b**, the lack of affinity may be due to the formation of weak interactions with the residues of the choline site. Thus, only two not parallel π-π interactions are observed with Tyr354 and Phe345 (Fig. 3a). The rest of the amino acids that make up the hydrophobic site where **b** is inserted do not contribute to the stabilization of the ligand. These amino acids are Tyr440, Trp420, Trp423 and Tyr437.

The low inhibitory power may also be due to the proximity of the compound to Asp306. This amino acid, which has been proposed as a catalytic base, performs a nucleophilic attack at the γ phosphate of the ATP and is phosphorylated. This ligand, which does not establish strong interactions with the residues of the active site, could easily be displaced from the hydrophobic pocket by the phosphorylated residue. Therefore, the choline can enter the choline pocket and become phosphorylated.

A similar mode of interaction must exist for compound **a**, since it shows affinity and inhibition values very similar to **b**. However, the quinoline ring of compounds **c**, **d** and **e**, as well as the phenyl of the *N*-methylaniline group present in **e** would lead to a diverse interaction profile in which aromatic systems would participate in the formation of additional interactions. As a result, the affinity for CK should be greater. However, according to the weak inhibition displayed, such additional interactions do not appear to be sufficient to keep them stably attached to the active site, so Asp306 phosphorylation could also cause their expulsion from the choline pocket.

The crystalline structure obtained for the compounds of the series C was formed by the complex CKα1/**o**, since the compound **n** had already been crystallized in recently published works [18] and the insolubility of the compounds **t** and **u** at high concentrations prevented their crystallization. Consequently, docking studies were also undertaken to explain the binding mode of the compound **u**, which in turn could be similar to that of the compound **t** given the structural similarity between the two.

According to the K_d values that were obtained for them, the affinity improved considerably with respect to the derivatives of the series A, this improvement being especially accentuated for the case of the pyridine derivatives.

In the crystal of the compound **o** (Fig. 3b) not only two molecules are observed at the site of the choline, but also parallel interactions π-π with the residues Tyr354 (molecule 1) and Tyr333 (molecule 2). In addition, the binding of molecule 1 is reinforced with unparallel π-π interactions with residues Phe435 and Tyr440. Trp420, Trp423 and Tyr437 residues are also part of the hydrophobic pocket where both molecules are inserted. Regarding these

Table 3
Inhibition of CKα1 activity by compounds a-v.

Compounds	Series	% Inhibition CKα1			IC_{50}[a] CKα1(μM)
		10 μM	30 μM	50 μM	
A		–	37.20 ± 8.00	–	nd
B		11,08 ± 1,62	19.57 ± 6.03	27,84 ± 1,72	nd
C	A	31,54 ± 8,07	35.02 ± 0,79	–	nd
D		35,81 ± 2.68	27.53 ± 5.41	38,7 ± 10,83	nd
E		23.08 ± 4.14	28.38 ± 0.14	18,58 ± 2,00	nd
F		25.42 ± 1.66	33.53 ± 0.26	nd	nd
G		–	–	nd	nd
H		8.07 ± 2.01	24.67 ± 2.42	nd	nd
I	B	–	–	nd	nd
J		–	24.92 ± 3.87	nd	nd
K		34.74 ± 3.71	52.68 ± 0.65	nd	nd
L		–	–	nd	nd
M		10.41 ± 2.54	14.50 ± 6.05	nd	nd
N		18.85 ± 1.47	26.45 ± 5,00	nd	nd
O		–	28,03 ± 1,06	nd	nd
P		–	–	nd	nd
Q	C	26.57 ± 5.54	30.19 ± 7.20	nd	nd
R		45.59 ± 3.06	53.03 ± 1.00	nd	nd
S		36.87 ± 2.56	46.28 ± 7.02	nd	nd
T		74.39 ± 0.93	94.44 ± 0.33	nd	6.74 ± 0.13
V		38.61 ± 5.30	76.00 ± 2.19	nd	12.55 ± 0.16

[a] IC_{50} compound concentration that inhibits 50% of the enzyme activity.

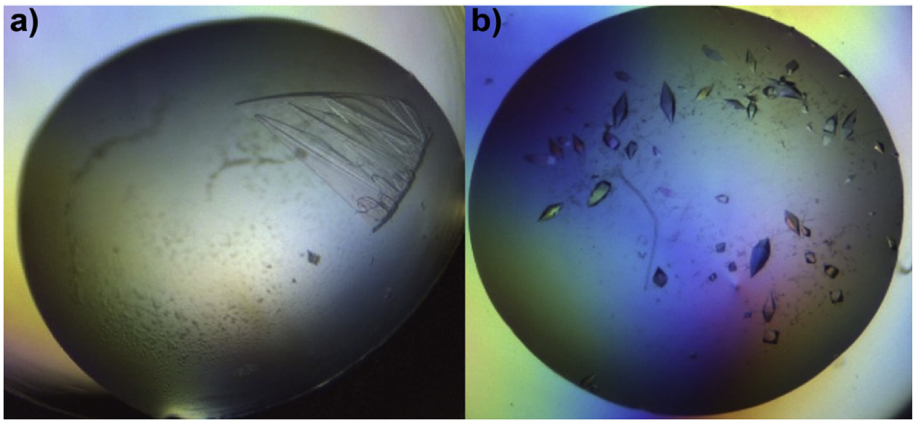

Fig. 2. Crystals from CKα1 selected for the compounds: a) compound **b**, b) compound **o**.

interactions, the bonding of the series C compounds is stronger than in the case of the series A compounds, probably thanks to the additional phenyl of the spacer. The result, therefore, is an improvement in affinity to CKα1 which is particularly notable in the case of pyridine derivatives and should lead to an increase in potency as inhibitors.

Crystallographic studies previously carried out with the compound **n** and other derivatives with dimethylaminopyridine as cation head (see Protein Data Bank, PDB IDs: 4BR3 and 4CGA) have shown that, although there is only one molecule occupying to the site of the choline, it has parallel interactions of the type π-π with the residues Tyr354, Phe435 and Trp420 (Fig. 4). This would explain the better affinity of the compound **n** with respect to its equivalent **a**. On the other hand, the comparison of the conformation adopted by the residues that make up the hydrophobic pocket where both compounds are inserted shows the remarkable rotation of Trp420 and Tyr333 residues that allow the accommodation od the second molecule of compound. So much so that it can be postulated that this conformational change would require an extra energy contribution that would be sufficient reason to think that CKα1 introduces molecule 1 (with an ordinary arrangement where it establishes interactions π-π parallel with Tyr354), and then molecule 2 (in the new cavity that Trp420 and Tyr333 open).

However, inhibition assays show that both **n** and **o** are not able to interrupt phosphocholine synthesis, so the interactions previously described do not seem to be sufficient to prevent the enzyme from expelling them from the active site.

3.5. Docking studies

Based on docking studies conducted with quinoline derivative **v** (Fig. 5), and depending on the observed K_d values, their binding mode to the choline binding site could occur in two different ways. In the first pose, the cationic head is inserted deep into the pocket of the choline, while in the second binding mode it is exposed to the solvent. However, in both cases, it is observed that their molecular recognition will be reinforced by extra interactions of the π-cation type, π-π parallel and non-parallel through the additional phenyl of the spacer, quinolinium group and *N*-methylaniline. This may explain their better affinity to **n** and **o** compounds, as well as

Table 4
X-ray crystal structure data collection and refinement statistics. Values in parentheses refer to the highest resolution shell. Ramachandran plot statistics were determined with PROCHECK.

	b	O
Space group	$P2_12_12_1$	$P4_32_12$
Wavelength (Å)	0.97	0.92
Resolution (Å)	20–2.15 (2.27–2.15)	61–1.80 (1.90–1.80)
Cell dimensions (Å)	*a* =*55.67*	*a* =*61.37*
	b = 118.77	*b* = 61.37
	c = 131.00	*c* = 221.07
Unique reflections	48047	40416
Completeness	99.9 (100)	99.9 (99.9)
R_{merge}	0.092 (0.715)	0.1 (0.653)
$I/\sigma(I)$	16.7 (3.1)	12.6 (2.8)
Redundancy	8.2 (8.2)	8.5 (8.7)
R_{work}/R_{free}	0.191/0.233	0.189/0.230
RMSD from ideal geometry, bonds (Å)	0.0086	0.011
RMSD from ideal geometry, angles (°)	1.527	1.385
<*B*> overall (Å^2)	39.65	22.06
<*B*> ligand (Å^2)	84.96	29.95
<*B*> solvent (Å^2)	44.74	37.07
<*B*> ethylene glycol (Å^2)	66.71	38.31
Ramachandran plot:		
Most favoured (%)	96.9	97.7
Additionally allowed (%)	2.9	2.30
Outliers (%)	0.1	0.00
PDB ID	**7A04**	**7A06**

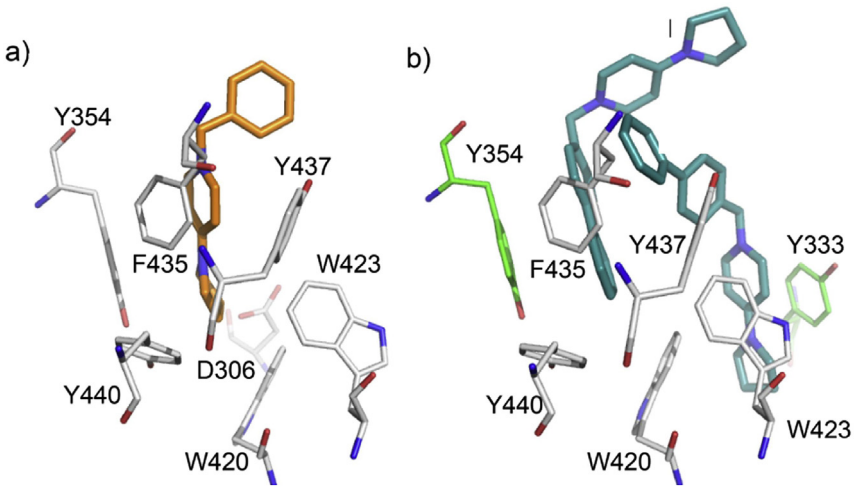

Fig. 3. a) Crystalline structure of the complex CKα1/**b**. b) Crystalline structure of the complex CKα1/**o**. The hydrophobic residues with which parallel interactions are formed π-π are shown in green. The rest of the residues that make up the hydrophobic pocket have been indicated in white. (For interpretation of the references to colour in this figure legend, the reader is referred to the Web version of this article.)

their **e** and **d** analogues. Specifically, the residues involved in the interaction π-cation are Tyr440 in the first pose, and Trp420 in the second. On the other hand, the parallel π-π interactions of the first pose would be established with residues Phe435 and Trp420, whereas according to the second pose, only the Tyr354 would be engaged in a π-π interaction. Finally, the non-parallel π-π interactions would form with Phe435, Tyr354 and Trp423 residues in the first pose, while in the second one Trp420, Phe435, Tyr440 and Trp428 residues seem to intervene.

Table 5 summarizes the interactions that the members of each series establish with the residues from the choline binding site.

*3.6. Comparison of the crystals of series **A** and **C** between themselves and with others previously published*

In this group of compounds, two types of ligands can be differentiated, **b** and **o**, which are introduced into the hill site in the same way as compound **14 (BR33)** [19] (Fig. 6). The superimposition however shows that the residues involved in the recognition of the three ligands are not the same. In this sense, the parallel interaction π-π that forms molecule 2 of compound **o** with Tyr333 is remarkable. This residue moves backwards to accommodate in the most stable way possible that molecule (Fig. 6d). In the case of **b**, it does not establish parallel π-π interactions with any amino acid, as previously indicated. On the other hand, compound **BR33** forms three π-π interactions, of which two are parallel with Tyr354 and Tyr333 residues. The amino acid Trp420 is responsible for the third interaction (Fig. 6b). Interestingly, molecule 1 of compound **o** superimposes its phenyl group attached directly to the cationic head with the phenyl of compound **BR33** (Fig. 6c). This arrangement allows it to establish parallel interactions π-π with Tyr354. Molecule 1 of **o** forms non-parallel π- π interactions with Phe435 and with Tyr440, respectively. If the poses of molecules 1 and 2 of the ligand **o** are compared, it can be seen that their biphenyl groups

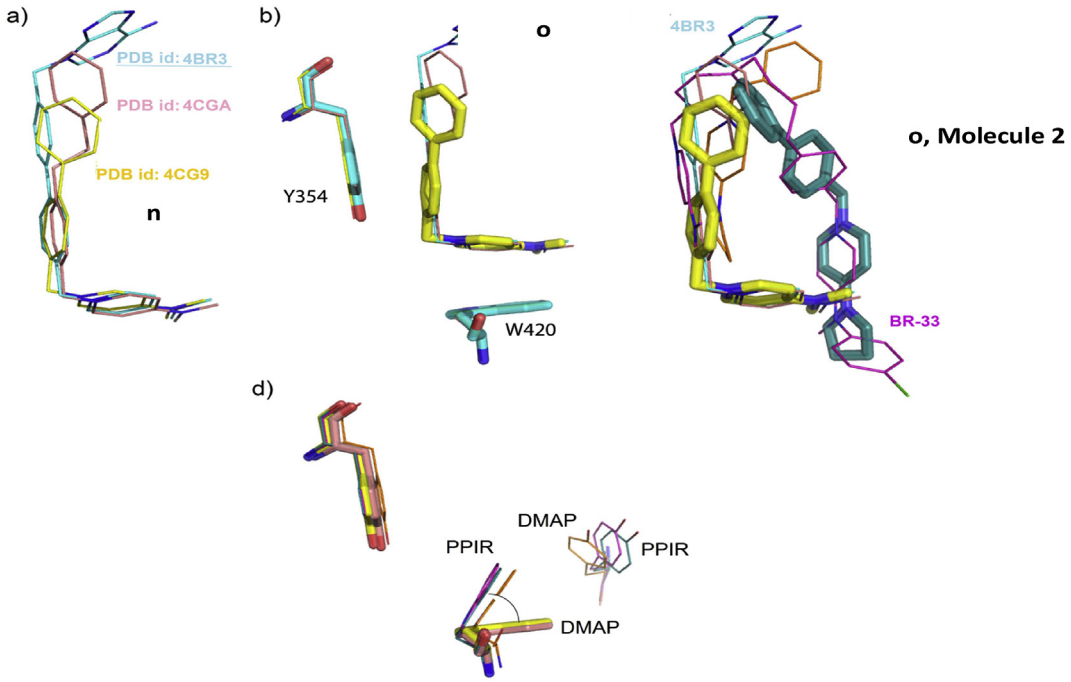

Fig. 4. Interactions of compound **n** and analogues with residues from the choline site. a) Superposition of compound **n** (PDB ID: 4CG9) and its derivatives from PDB code crystals: 4CGA and 4BR3. b) Residues from the active site with which they form parallel interactions π-π. c) Superposition of **n** and derivatives with **o** and the compound BR-33. d) Conformational changes of the residues of the active site (Trp420 and Tyr 333) against the derivatives of dimethylaminopyridine (DMAP) and pyrrolidinopyridine (PPIR).

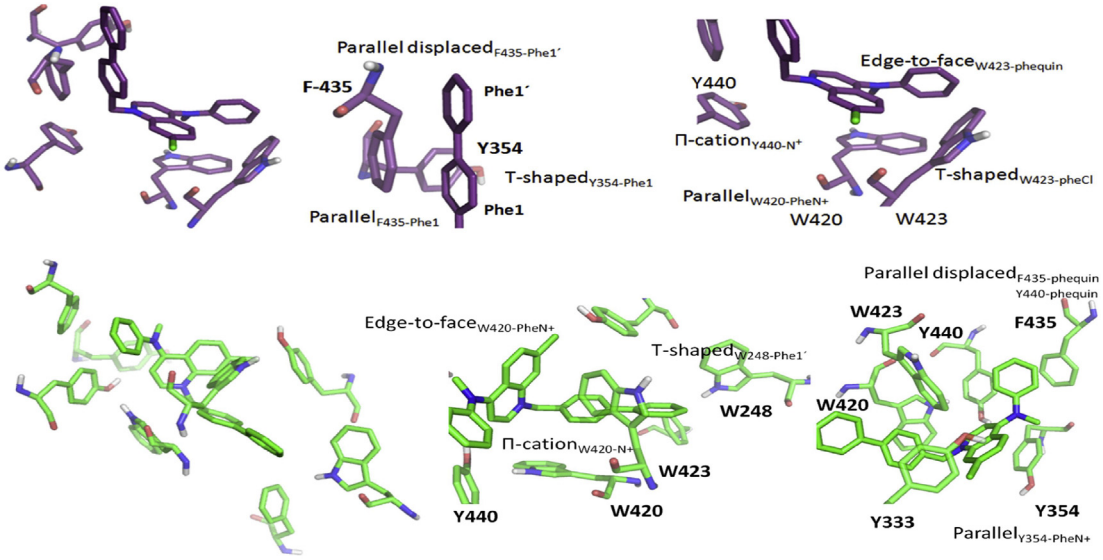

Fig. 5. First and second pose adopted by the compound **v** in the docking studies performed. All interactions established are indicated in the figures.

Table 5
Interaction profile of the members of each series. Table 5.

Compounds		n-p	s-v	b
Π-π	Parallel	W420, F435, Y354	Y354 (molecule 1), Y333 (molecule 2)	–
Interactions	Unparallel	W423	F435 (molecule 1, Phe', Y440 (molecule 1, Phe')	Y354, F345
Hydrophobic pocket		Y333, Y437, Y440	W420, W423, Y437	W420, W423, Y437, Y440
Relevant aspects		Y354 helps to stabilize all ligands regardless of the chemical nature of the spacer and cation head		

are arranged parallel to each other (Fig. 7), in such a way that the formation of non-parallel π-π interactions between them is favoured.

In conclusion, each of these interaction profiles is responsible for a higher K_d value than that of the quinoline derivatives. In view of the above, this observation may respond to the formation of fewer parallel interactions π-π.

The typical disposition of dimethylaminopyridine derivatives (DMAP) at the choline binding site involves the formation of three parallel π-π interactions with Trp420, Tyr354 and Phe435 residues (Fig. 4). All of these are the cause of the stronger affinity that DMAP derivatives generally show with pyrrolidinopyridine (PPIR). An interaction between the amino acid Trp423 and the pyridine ring of compound **n** can also be seen at π-π The DMAP fragment is superimposed in all cases, however, the rest of the molecule is arranged differently depending on the spacer (Fig. 4). This confirms once again that the part of the molecule that is really important for interacting with the CK protein is the pharmacophore that has been previously proposed.

The comparison of the residues orientation involved in the interaction of DMAP and PPIR derivatives, showed the turnaround of the Trp420 and Try333 residues to facilitate the binding of PPIR derivatives (Fig. 4d).

3.7. Inhibition uptake of choline assays

Since it has been previously demonstrated that some CKα1 inhibitors, in addition to their effects, are able to reduce choline uptake [28–30], we decided to investigate whether the test compounds are also capable of inhibiting choline uptake, as described in previous research conducted by our group [14–16]. The **A** series inhibitors have not been tested as they have lower antiproliferative activity and lower capacity to inhibit the CKα1 enzyme. Compounds **f**, **h** and **i** were chosen from the **B** series. The first two inhibit the enzyme by 33% and 8%, respectively, while the third is unable to inhibit CKα1 activity (Table 3). Among those three inhibitors, only compound **f** shows antiproliferative activity in HT-29 cells. As shown in Table 6, none of these three compounds potently inhibits choline uptake in either HT-29 cells or HepG2 cells (the latter was chosen to corroborate results in a different cell line). The results highlighted the hypothesis that the antiproliferative effect obtained with B series compounds is mainly due to the inhibition of CKα1 activity.

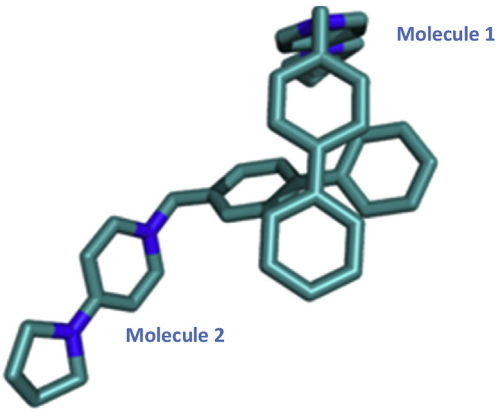

Fig. 7. Cross arrangement of the two molecules of **o**.

Conversely, within the **C** series, we observed that the antiproliferative activity of compounds **o** and **p** directly correlates with the inhibition in choline uptake, while for the compounds **t** and **v**, the antiproliferative action is due both to the inhibition of CKα1 and choline uptake. Further investigations are needed to better determine the relationship between the degree of inhibition of choline uptake and the antiproliferative effect, as well as the correlation with the compound structures, without ruling out that other mechanisms may contribute to antiproliferative SAR.

3.8. Compound *t* induce G0/G1 arrest of the cell cycle and apoptosis through the mitochondrial pathway

Previous reports indicated that molecules that are able to inhibit choline kinase significantly inhibits cell growth in different tumoral cell lines, in a concentration dependent manner, due to a G_0/G_1 arrest of the cell cycle [13,16,20].

In this context we evaluated the cell cycle after treatment with compound **t**, one of the most active derivatives in two cancer cell lines (HeLa and HT-29). As depicted in Fig. 8, the drug induces a significant accumulation in G0/G1 phase in both cell lines, although highly pronounced in HT-29 cells, accompanied by the consequent decrease of the S-phase, in a concentration-dependent manner (Fig. 8, Panels A and B).

To evaluate the mode of cell death induced by compound **t**, we

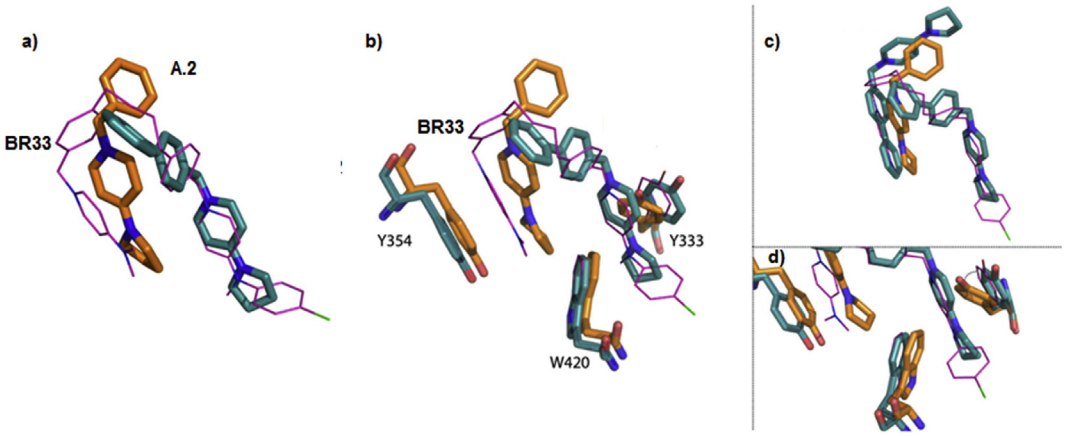

Fig. 6. a) Superposition of the crystalline structures of compounds **b** (orange), **o** (blue) and **BR33** (magenta). b) Some of the residues with which π-π interactions are formed. c) Superposition of the pyridinium groups of the two molecules of compound **o** with the pyridinium group of compound **BR33** and proximity with the pyridinium of **b**. d) Backward rotation of Tyr333 to accommodate molecule 2 of compound **o** and the N-methylaniline group of **BR33**. (For interpretation of the references to colour in this figure legend, the reader is referred to the Web version of this article.)

Table 6
Inhibition of [3H]choline uptake by compounds **a-v** in HT-29 and HepG2 cells. Values of percentage of inhibition of choline uptake in HT-29 and HepG2 cells.

Compounds	GI_{50} (μM) HT-29	Choline uptake HT-29% inhibition		Choline uptake HepG2 % inhibition	
		10 μM	30 μM	10 μM	30 μM
A	>100	nd	nd	nd	nd
B	38.0 ± 0.6	nd	nd	nd	nd
d	4.6 ± 0.14	nd	nd	nd	nd
e	4.5 ± 0.16	nd	nd	nd	nd
f	11.2 ± 0.37	14.3 ± 1.15	22.7 ± 1.06	11.7 ± 0.8	16.9 ± 0.8
h	>100	9.1 ± 0.99	2.4 ± 1,29	5.1 ± 2.4	17.7 ± 2.2
I	>100	17.6 ± 0.76	21.6 ± 3.8	14.3 ± 4.2	15.1 ± 1.7
N	0.29 ± 0.01	nd	nd	nd	nd
O	0.16 ± 0.07	56.7 ± 1.6	79.5 ± 0.33	70.3 ± 0.77	84.3 ± 0.79
P	0.23 ± 0.03	78.4 ± 0.20	95.0 ± 0.34	83.3 ± 0.71	94.8 ± 0.24
S	0.04 ± 0.003	nd	nd	nd	nd
T	0.09 ± 0.009	86.9 ± 1.08	96.7 ± 0.14	88.2 ± 0.84	95.5 ± 0.21
V	0.85 ± 0.12	85.5 ± 1.00	93.3 ± 0.55	87.2 ± 0.03	94.8 ± 0.34

performed a bi-parametric cytofluorimetric analysis using propidium iodide (PI) and annexin-V-FITC, which stain DNA and phosphatidylserine (PS) residues, respectively. As showed in Fig. 8 (panels C and E), **t** induces a dose- and time-dependent increase in apoptotic cells in both cell lines cell lines. In order to evaluate the type of apoptosis induced by the compound, we analyzed the variation of mitochondrial potential following treatment. It is well known that many drugs cause apoptosis through the so-called intrinsic pathway in which mitochondria play an essential role in the propagation of apoptosis [31]. In particular at an early stage, apoptotic stimuli alter the mitochondrial transmembrane potential ($\Delta\psi_{mt}$) that ultimately leads to apoptosis. With this aim we treated both HeLa and HT-29 cell with **t** and after 24 h the dissipation of $\Delta\psi_{mt}$ was monitored by flow cytometry in the presence of the fluorescent dye JC-1. As depicted in Fig. 8 **(panels D and F)**, compound **t** is able to significantly reduce mitochondrial potential early after treatment and in a concentration dependent manner in both the two cell lines investigated.

4. Conclusions

In this paper we have presented a series of compounds (**a-v**) that were initially designed and synthesized to validate our previously described pharmacophore model (RRRPN). These compounds were tested against four tumor cell lines with good or moderate antiproliferative properties, where the most complex structures (series **C**) turned out to be the best choline kinase inhibitors. The affinity (K_d), selectivity (versus β isoform) and degree of inhibition were evaluated on the isolated human choline kinase. Our results showed a poor enzyme inhibition, which do not correlate with antiproliferative activity. Indeed, we observed that the compounds are also capable of inhibiting the uptake of choline and this effect could in part contribute to their antiproliferative activity. However, it is still not ruled out that these compounds could also be involved in other mechanisms related to the hitherto underestimated role of choline kinase alpha in protein-protein interactions. So, further studies are needed to clarify if our compounds have the additional benefit of disrupting the surface of the protein, regardless of their action on enzymatic activity.

5. Experimental protocols

5.1. Chemistry

5.1.1

Materials and Methods.

Melting points were taken in open capillaries on a Stuart Scientific SMP3 electrothermal melting-point apparatus and were uncorrected. Analytical thin-layer chromatography (TLC) was performed using Merck Kieselgel 60 F254 aluminium plates and visualized by UV light or iodine. All evaporation occurred *in vacuo* with a Büchi rotary evaporator and the pressure controlled by a Vacuubrand CVCII apparatus. For flash chromatography, Merck silica gel 60 with a particle size of 0.040–0.063 mm (230–400 mesh ASTM) was used: 500 MHz ^{1}H and 126 MHz ^{13}C NMR Varian Direct Drive; a 400 MHz ^{1}H and 101 MHz ^{13}C NMR Varian Direct Drive spectrometers at room temperature. Chemical shifts (δ) are quoted in parts per million (ppm) and are referenced to the residual solvent peak. Spin multiplicities are given as s (singlet), bs (broad singlet), d (doublet), t (triplet), ddd (doublet doublet doublet), dd (doublet doublet), dt (doublet triplet), q (quadruplet) and m (multiplet). High-resolution NanoAssisted Laser Desorption/Ionization (NALDI-TOF) or Electrospray Ionization (ESI-TOF) mass spectra were carried out on a Bruker Autoflex or a Waters LCT Premier Mass. Organic solutions were dried over anhydrous Na_2SO_4. Solvents and reagents that are commercially available were purchased from Aldrich (Sigma-Aldrich) or Alfa Aesar (Johnson Matthey Company) and were used without further purification unless otherwise noted.

5.1.2. General procedure for the synthesis of the target compounds

To a prepared solution of 4-Bromobenzyl, 1-(bromomethyl)-4-(trifluoromethyl)benzene or 4-(bromomethyl)-1,1′-biphenyl in butanone or acetonitrile as solvent, was added the corresponding intermediates 1–3 and (7-chloro)-4-subtitutedquinoline 4 [3,6,7] (in a molar ratio of 1:1). The reaction was performed in a sealed tube a under microwave irradiation (140 °C, 28–33 min). Target compounds **a-v** were isolated after chromatography flash purification or simple filtration and wash with diethyl ether.

*5.1.2.1. 1-benzyl-4-(dimethylamino)pyridin-1-ium bromide (**a**).* Following general procedure, after workup as described previously, compound **a** was isolated as a white solid. Yield: 88%, mp 210–212 °C. ^{1}H NMR (500 MHz, CD_3OD) δ 3.26 (s, 6H), 5.38 (s, 2H), 7.01 (d, $J = 7.8$ Hz, 2H), 7.44–7.38 (m, 5H), 8.23 (d, $J = 7.8$ Hz, 2H). ^{13}C NMR (125 MHz, CD_3OD) δ 38.98 (2C), 60.38 (1C), 107.74 (2C), 127.93 (2C), 128.88 (1C), 129.06 (2C), 134.79 (1C), 141.73 (2C), 156.75 (1C). HRMS-m/z[M − Br]$^+$ calcd for $C_{14}H_{17}N_2^+$ [M − Br]$^+$: 213.1392; found, 213.1387.

*5.1.2.2. 1-benzyl-4-(pyrrolidin-1-yl)pyridin-1-ium bromide (**b**).* Following general procedure, after workup as described previously, compound **b** was isolated as a white solid. Yield: 82%, mp 226–228 °C. ^{1}H NMR (500 MHz, CD_3OD) δ 2.12 (q, $J = 7.0$, 4H), 3.56

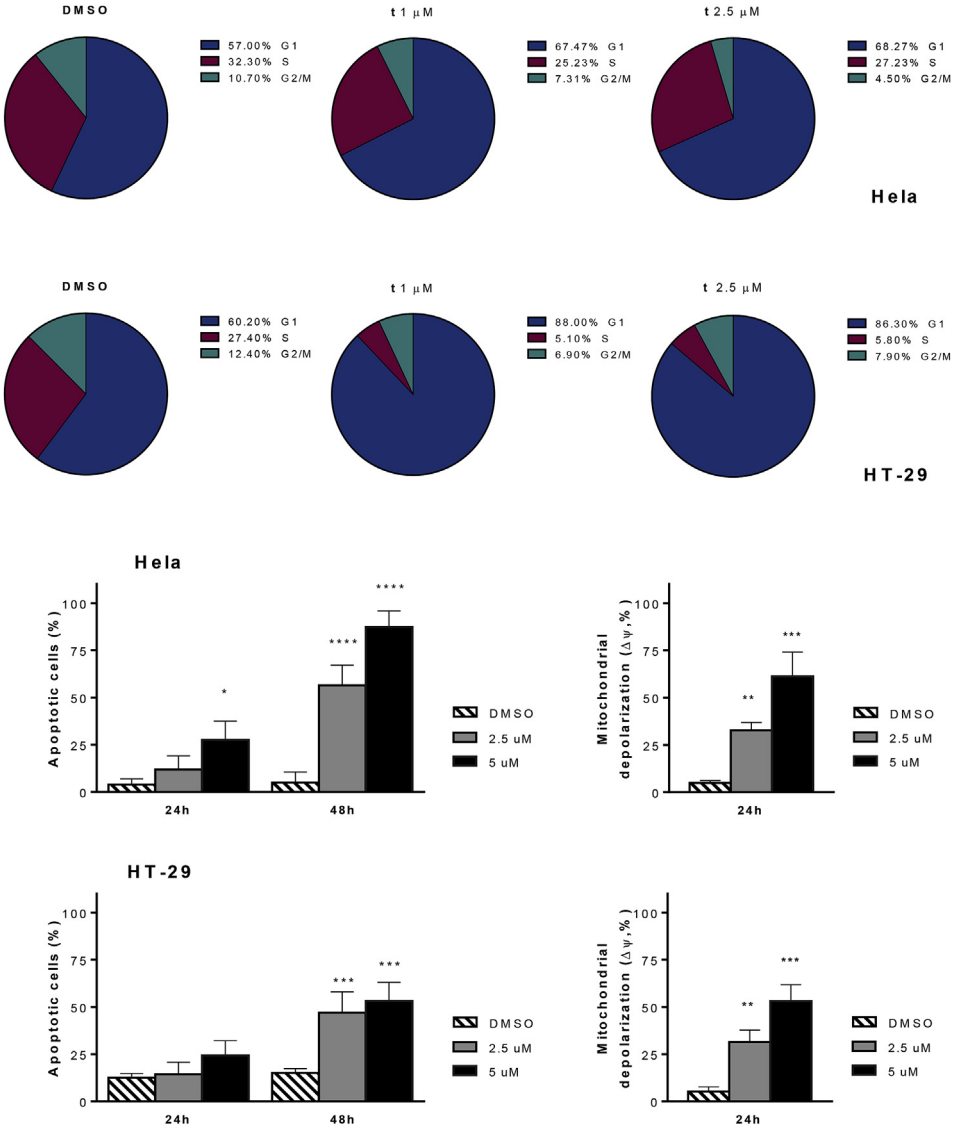

Fig. 8. Percentage of cells in each phase of the cell cycle in HeLa (Panel A) and Jurkat cells (Panel B) treated with compound **t** at the indicated concentrations for 24 h. Cells were fixed and labelled with PI and analyzed by flow cytometry as described in the Experimental Section. Data are presented as mean ± SEM of three independent experiments. Flow cytometric analysis of apoptotic cells after treatment of HeLa (Panels A and B) and Jurkat (Panels C and D) cells with **t** at the indicated concentrations after incubation for 24 (Panels A and C) or 48 h (Panels B and D). The cells were harvested and labelled with annexin-V-FITC and PI and analyzed by flow cytometry.
Assessment of mitochondrial membrane potential ($\Delta\psi_{mt}$) (Panel A) and production of ROS (Panel B) after treatment of HeLa cells with compound **t**. Cells were treated with the indicated concentration of compound for 3, 6, 12 and 24 h and then stained with the fluorescent probe JC-1 for analysis of mitochondrial potential or with 2,7-dichlorodihydrofluorescein diacetate (H_2-DCFDA).

(t, J = 6.9 Hz, 4H), 5.37 (s, 2H), 6.87 (d, J = 7.7 Hz, 2H), 7.38–7.45 (m, 5H), 8.21 (d, J = 7.7 Hz, 2H). ^{13}C NMR (125 MHz, CD_3OD) δ 24.76 (2C), 48.30 (2C), 60.38 (1C), 108.28 (2C), 127.84 (2C), 128.81 (1C), 129.00 (2C), 134.96 (1C), 141.51 (2C), 153.84 (1C). HRMS-m/z $[M - Br]^+$ calcd for $C_{16}H_{19}N_2^+$: 239.1548; found, 239.1542.

*5.1.2.3. 1-benzyl-7-chloro-4-(pyrrolidin-1-yl)quinolin-1-ium bromide. (**c**).* Following general procedure, after workup as described previously, compound **c** was isolated as a white solid. Yield: 79%, mp 256–258 °C. ^{1}H NMR (401 MHz, CD_3OD) δ 2.16 (s, 4H), 4.01 (s, 4H), 5.76 (s, 2H), 6.86 (d, J = 7.6 Hz, 2H), 7.23 (d, J = 7.0 Hz, 1H), 7.41–7.26 (m, 2H), 7.63 (pt, J = 7.6 Hz, 1H), 7.88–7.80 (pt, J = 7.5 Hz, 1H), 7.92 (d, J = 8.8 Hz, 1H), 8.51 (d, J = 7.6 Hz, 1H), 8.61 (d, J = 8.6 Hz, 1H). ^{13}C NMR (101 MHz, CD_3OD) δ (126 MHz, CD_3OD): 26.50 (2C), 54.44 (2C), 58.58 (1C), 103.85 (1C), 118.84 (1C), 119.28 (1C), 126.87 (1C), 127.82 (2C), 129.73 (1C), 130.37 (2C), 131.16 (1C), 135.79 (1C), 140.94 (1C), 141.61 (1C), 146.34 (1C), 157.10 (1C). HRMS-m/z $[M - Br]^+$ calcd for $C_{20}H_{20}ClN_2^+$: 323.1310; found, 323.1315.

*5.1.2.4. 4-(azepan-1-yl)-1-benzyl-7-chloroquinolin-1-ium bromide (**d**).* Following general procedure, after workup as described previously, compound **d** was isolated as a white solid. Yield: 53%, mp 225–227 °C. ^{1}H NMR (400 MHz, CD_3OD) δ 1.76–1.72 (m, 4H), 2.08–2.01 (m, 4H), 4.09 (t, J = 5.5 Hz, 4H), 5.80 (s, 2H), 7.10 (d, J = 3.8 Hz, 1H), 7.28–7.30 (m, 2H), 7.43–7.35 (m, 3H), 7.64 (dd, J = 1.6, 9.2 Hz, 1H), 7.98 (d, J = 2.04 Hz, 1H), 8.37 (d, J = 9.2 Hz, 1H), 8.51 (d, J = 7.8 Hz, 1H). ^{13}C NMR (150 MHz, CD_3OD) δ 27.63 (2C), 28.29 (2C), 55.23 (2C), 58.44 (1C), 104.25 (1C), 118.85 (1C), 118.94 (1C), 126.53 (1C), 127.86 (2C), 129.76 (1C), 130.38 (2C), 131.52 (1C), 135.68 (1C), 140.94 (1C), 142.06 (1C), 146.16 (1C), 160.68 (1C). HRMS-m/z $[M - Br]^+$ calcd for $C_{22}H_{24}N_2Cl^+$: 351.1628; found, 351.1631.

*5.1.2.5. 1-benzyl-7-chloro-4-(methyl(phenyl)amino)quinolin-1-ium bromide (**e**).* Following general procedure, after workup as described previously, compound **e** was isolated as a white solid. Yield: 87%, mp 259–261 °C. ^{1}H NMR (600 MHz, CD_3OD) δ 2.46 (s, 3H), 5.82 (s, 2H), 6.89 (d, J = 7.4 Hz, 1H), 7.30–7.28 (m, 2H), 7.44–7.37 (m, 8H), 7.80 (dd, J = 1.9, 9.0 Hz, 1H), 8.08 (d, J = 1.9 Hz, 1H), 8.55 (d, J = 7.5 Hz, 1H), 8.62 (d, J = 9.0 Hz, 1H). ^{13}C NMR (125 MHz, CD_3OD) δ 19.82 (1C), 57.64 (1C), 100.48 (1C), 117.12 (1C), 118.36 (1C), 125.17 (2C), 125.63 (1C), 126.38 (2C), 127.71 (1C), 128.48 (1C), 129.03 (2C), 129.86 (1C), 130.47 (2C), 134.20 (1C), 138.52 (1C), 139.38 (1C), 140.67 (1C), 147.65 (1C), 155.98 (1C). HRMS-m/z [M − Br]$^+$ calcd for $C_{23}H_{20}N_2Cl^+$: 359.1315; found, 359.1306.

*5.1.2.6. 4-(dimethylamino)-1-(4-(trifluoromethyl)benzyl)pyridin-1-ium bromide (**f**).* Following general procedure, after workup as described previously, compound **f** was isolated as a white solid. Yield: 75%, mp 216–218 °C. ^{1}H NMR (300 MHz, CD_3OD) δ 3.37 (m, 6H), 5.50 (s, 2H), 7.03 (d, J = 7.6 Hz, 2H), 7.56 (d, J = 8.0 Hz, 2H), 7.74 (d, J = 8.2 Hz, 2H), 8.26 (d, J = 7.6 Hz, 2H). ^{13}C NMR (75 MHz, CD_3OD) δ 40.36 (2C), 60.49 (1C), 109.09 (2C), 127.20 (2C), 129.59 (2C), 132.50 (1C), 132.52 (1C), 140.13 (1C), 142.74 (2C), 157.66 (1C). HRMS-m/z [M − Br]$^+$ calcd for $C_{15}H_{16}N_2F_3^+$: 281.1266; found, 281.1272.

*5.1.2.7. 4-(pyrrolidin-1-yl)-1-(4-(trifluoromethyl)benzyl)pyridin-1-ium bromide (**g**).* Following general procedure, after workup as described previously, compound **g** was isolated as a white solid. Yield: 84%, mp 74.8–76.3 °C. ^{1}H NMR (300 MHz, CD_3OD) δ 2.14 (m, 4H), 3.56 (m, 4H), 5.50 (s, 2H), 6.87 (d, J = 7.6 Hz, 2H), 7.58 (d, J = 8.0 Hz, 2H), 7.76 (d, J = 8.2 Hz, 2H), 8.25 (d, J = 7.6 Hz, 2H). ^{13}C NMR (75 MHz, CD_3OD) δ 26.17 (2C), 49.15 (2C), 60.98 (1C), 109.69 (2C), 125.39 (1C), 127.31 (2C), 129.67 (2C), 130.60 (1C), 140.76 (1C), 143.22 (2C), 154.99 (1C). HRMS-m/z[M − Br]$^+$ calcd for $C_{17}H_{18}N_2F_3^+$: 307.1422; found, 307.1417.

*5.1.2.8. 1-(4-(trifluoromethyl)benzyl)quinuclidin-1-ium bromide (**h**).* Following general procedure, after workup as described previously, compound **h** was isolated as a white solid. Yield: 71%, mp 238.3–239 °C. ^{1}H NMR (300 MHz, CD_3OD) δ 2.03 (m, 6H), 2.18 (m, 1H) 3.53 (m, 6H), 4.53 (s, 2H), 7.78 (d, J = 8.1 Hz, 2H), 7.86 (d, J = 8.1 Hz, 2H). ^{13}C NMR (75 MHz, CD_3OD) δ 21.48 (1C), 25.05 (3C), 56.22 (3C), 67.65 (1C), 127.25 (2C), 133.18 (1C), 133.45 (1C), 134.42 (1C), 135.20 (2C). HRMS-m/z[M − Br]$^+$ calcd for $C_{15}H_{19}NF_3^+$: 270.1470; found, 270.1475.

*5.1.2.9. 1-(4-(trifluoromethyl)benzyl)-3-hydroxy-quinuclidin-1-ium bromide (**i**).* Following general procedure, after workup as described previously, compound **i** was isolated as a white oil. Yield: 68%. ^{1}H NMR (400 MHz, CD_3OD) δ 2.03 (m, 2H), 2.19 (m, 1H) 3.21 (dd, J = 12.0 Hz, 1H), 3.45–3.37 (m, 5H), 3.74 (m. 1H), 4.21 (m, 1H), 4.55 (d, J = 8.1 Hz, 1H), 4.59 (s, 2H), 7.76 (d, J = 8.1 Hz, 2H), 7.85 (d, J = 8.1 Hz, 2H). ^{13}C NMR (100 MHz, CD_3OD) δ 18.85 (1C), 22.44 (1C), 28.39 (1C), 54.80 (1C), 56.21 (1C), 64.68 (1C), 65.15 (1C), 67.58 (1C), 127.16 (2C), 132.60 (1C), 133.43 (1C), 133.69 (1C), 135.02 (2C). HRMS-m/z[M − Br]$^+$ calcd for $C_{15}H_{19}NF_3^+$: 286.1419; found, 286.1413.

*5.1.2.10. 7-chloro-4-(pyrrolidin-1-yl)-1-(4-(trifluoromethyl)benzyl) quinolin-1-ium bromide (**j**).* Following general procedure, after workup as described previously, compound **j** was isolated as a yellow solid. Yield: 91%, mp 221–223 °C. ^{1}H NMR (300 MHz, CD_3OD) δ 2.22 (m, 4H), 4.16 (m, 4H), 5.91 (s, 2H), 6.95 (d, J = 7.7 Hz, 1H), 7.47 (d, J = 8.1 Hz, 2H), 7.79–7.64 (m, 3H), 7.93 (d, J = 1.9 Hz, 1H), 8.55 (d, J = 7.7 Hz, 1H), 8.65 (d, J = 9.3 Hz, 1H). ^{13}C NMR (101 MHz, CD_3OD) δ 25.27 (2C), 56.40 (2C), 65.45 (1C), 102.16 (1C), 102.62 (1C), 117.14 (1C), 117.86 (1C), 125.57 (1C), 125.79 (1C), 126.95 (2C), 128.97 (1C), 129.85 (2C), 139.00 (1C), 139.81 (1C), 140.12 (1C), 144.96 (1C), 155.81 (1C). HRMS-m/z[M − Br]$^+$ calcd for $C_{21}H_{19}ClN_2F_3^+$: 391.1185; found, 391.1185.

*5.1.2.11. 4-(azepan-1-yl)-7-chloro-1-(4-(trifluoromethyl)benzyl)quinolin-1-ium bromide (**k**).* Following general procedure, after workup as described previously, compound **k** was isolated as a white solid. Yield: 78%, mp 146–148 °C. ^{1}H NMR (300 MHz, CD_3OD) δ 1.74–1.70 (m, 4H), 2.00–2.10 (m, 4H), 4.07 (t, J = 5.6 Hz, 4H), 5.87 (s, 2H), 7.12 (d, J = 7.8 Hz, 1H), 7.45 (d, J = 8.1 Hz, 2H), 7.62 (dd, J = 9.2, 2.0 Hz, 1H), 7.70 (d, J = 8.0 Hz, 2H), 7.91 (d, J = 2.0 Hz, 1H), 8.38 (d, J = 9.2 Hz, 1H), 8.52 (d, J = 7.8 Hz, 1H). ^{13}C NMR (101 MHz, CD_3OD) δ 28.70 (4C), 54.69 (2C), 57.13 (2C), 103.70 (1C), 118.00 (1C), 118.35 (1C), 126.07 (1C), 126.59 (1C), 126.62 (1C), 127.83 (2C), 131.05 (2C), 139.75 (1C), 140.61 (1C) 141.45 (1C), 145.68 (1C), 160.22 (1C). HRMS-m/z[M − Br]$^+$ calcd for $C_{23}H_{23}ClN_2F_3^+$: 419.1502; found, 419.1512.

*5.1.2.12. 7-chloro-4-(methyl(phenyl)amino)-1-(4-(trifluoromethyl) benzyl)quinolin-1-ium bromide (**l**).* Following general procedure, after workup as described previously, compound **l** was isolated as a yellow solid. Yield: 81%, mp 227–229 °C. ^{1}H NMR (500 MHz, CD_3OD) δ 2.44 (s, 3H), 5.95 (s, 2H), 6.91 (d, J = 7.5 Hz,1H), 7.24–7.53 (m, 7H), 7.71 (d, J = 8.1 Hz, 2H), 7.81 (dd, J = 9.0, 1.9 Hz, 1H), 8.05 (d, J = 2.0 Hz, 1H), 8.62 (dd, J = 12.6, 8.3 Hz, 2H). ^{13}C NMR (101 MHz, CD_3OD) δ (126 MHz, CD_3OD): 19.75 (1C), 56.85 (1C), 100.73 (1C), 117.20 (1C), 118.04 (2C), 125.18 (2C), 125.79 (3C), 126.95 (2C), 127.84 (1C), 130.48 (3C), 133.82 (1C), 138.64 (1C), 138.82 (1C), 139.33 (1C), 140.95 (1C), 147.87 (1C), 156.15 (1C). HRMS-m/z[M − Br]$^+$ calcd for $C_{24}H_{19}ClN_2F_3^+$: 427.1189; found, 427.1195.

*5.1.2.13. 7-chloro-4-((4-chlorophenyl)(methyl)amino)-1-(4-(trifluoromethyl)benzyl)quinolin-1-ium bromide (**m**).* Following general procedure, after workup as described previously, compound **m** was isolated as a yellow solid. Yield: 88%, mp 298–300 °C. ^{1}H NMR (300 MHz, CD_3OD) δ 3.83 (s, 3H), 6.04 (s, 2H), 7.47–7.33 (m, 4H), 7.52 (dd, J = 12.5, 8.5 Hz, 4H), 7.63 (d, J = 9.3 Hz, 1H), 7.73 (d, J = 8.1 Hz, 2H), 8.04 (d, J = 1.9 Hz, 1H), 8.89 (d, J = 7.5 Hz, 1H). ^{13}C NMR (101 MHz, CD_3OD) δ 44.54 (1C), 57.33 (1C), 106.29 (1C), 118.03 (1C), 118.40 (1C), 125.86 (1C), 125.90 (1C), 126.51 (1C), 127.13 (4C), 129.56 (1C), 130.66 (4C), 133.85 (2C), 138.50 (1C), 138.53 (1C), 145.99 (1C), 147.41 (1C), 158.57 (1C). HRMS-m/z[M − Br]$^+$ calcd for $C_{24}H_{18}ClN_2F_3^+$: 461.0799; found, 461.0803.

*5.1.2.14. 1-([1,1′-biphenyl]-4-ylmethyl)-4-(dimethylamino)pyridin-1-ium bromide (**n**).* Following general procedure, after workup as described previously, compound **n** was isolated as a white solid. Yield: 95%, mp 222–224 °C. ^{1}H NMR (500 MHz, CD_3OD) δ 3.26 (s, 6H), 5.42 (s, 2H), 7.02 (d, J = 7.8 Hz, 2H), 7.36 (t, J = 7.4 Hz, 1H), 7.51–7.40 (m, 4H), 7.61 (d, J = 7.4 Hz, 2H), 7.69 (d, J = 8.2 Hz, 2H), 8.26 (d, J = 7.8 Hz, 2H). ^{13}C NMR (125 MHz, CD_3OD) δ 40.36 (2C), 61.47 (1C), 109.14 (2C), 127.99 (2C), 128.86 (1C), 128.92 (2C), 129.90 (2C), 130.00 (2C), 135.07 (1C), 141.36 (1C), 143.11 (2C), 143.48 (1C), 158.04 (1C). HRMS-m/z[M − Br]$^+$ calcd for $C_{20}H_{21}N_2^+$: 289.1705; found, 289.1698.

*5.1.2.15. 1-([1,1′-biphenyl]-4-ylmethyl)-4-(pyrrolidin-1-yl)pyridin-1-ium bromide (**o**).* Following general procedure, after workup as described previously, compound **o** was isolated as a white solid. Yield: 94%, mp 196–198 °C. ^{1}H NMR (300 MHz, CD_3OD) δ 2.12 (q, J = 6.8 Hz, 4H), 3.56 (t, J = 6.9 Hz, 4H), 5.41 (s, 2H), 6.87 (d, J = 7.8 Hz, 2H), 7.36 (t, J = 7.4 Hz, 1H), 7.48–7.43 (m, 4H), 7.61 (d, J = 8.2 Hz, 2H), 7.68 (d, J = 8.4 Hz, 2H), 8.24 (d, J = 7.8 Hz, 2H). ^{13}C NMR (125 MHz, CD_3OD) δ 24.71 (2C), 48.70 (2C), 60.08 (1C), 108.28 (2C), 126.57 (2C), 127.43 (1C), 127.47 (2C), 128.48 (2C), 128.58 (2C), 133.78

(1C), 139.94 (1C), 141.62 (2C), 141.98 (1C), 153.77 (1C). HRMS-m/z [M − Br]$^+$ calcd for $C_{22}H_{23}N_2^+$: 315.1861; found, 315.1863.

*5.1.2.16. 1-([1,1′-biphenyl]-4-ylmethyl)-4-((4-chlorophenyl)(methyl) amino)pyridin-1-ium bromide (**p**).* Following general procedure, after workup as described previously, compound **p** was isolated as a white solid. Yield: 84%, mp 199−201 °C. ^{1}H NMR (401 MHz, CD_3OD) δ 3.52 (s, 3H), 5.46 (s, 2H), 6.93 (d, *J* = 7.9 Hz, 2H), 7.41−7.29 (m, 3H), 7.46−7.39 (m, 3H), 7.49 (d, *J* = 8.2 Hz, 2H), 7.63−7.53 (m, 3H), 7.67 (d, *J* = 8.3 Hz, 2H), 8.33 (d, *J* = 7.9 Hz, 2H). ^{13}C NMR (125 MHz, CD_3OD) δ (126 MHz, CD_3OD): 39.94 (1C), 60.50 (1C), 108.98 (2C), 126.57 (2C), 127.46 (2C), 127.53 (2C), 127.97 (2C), 128.58 (2C), 128.61 (2C), 130.68 (2C), 133.38 (1C), 134.31 (1C), 139.99 (1C), 142.00 (1C), 142.16 (1C), 142.42 (1C), 157.10 (1C). HRMS-m/z[M − Br]$^+$ calcd for $C_{25}H_{22}N_2Cl^+$: 385.1472; found, 385.1475.

*5.1.2.17. 1-([1,1′-biphenyl]-4-ylmethyl)quinuclidin-1-ium bromide (**q**).* Following general procedure, after workup as described previously, compound **q** was isolated as a white solid. Yield: 71%, mp 281−283 °C. ^{1}H NMR (300 MHz, CD_3OD) δ 7.78 (d, *J* = 8.3 Hz, 2H), 7.66 (dd, *J* = 8.4, 1.1 Hz, 2H), 7.59 (d, *J* = 8.3 Hz, 2H), 7.53−7.43 (m, 2H), 7.44−7.33 (m, 1H), 4.43 (s, 2H), 3.62−3.41 (m, 6H), 2.17 (m, 1H), 2.04−1.98 (m, 6H). . ^{13}C NMR (151 MHz, CD_3OD): δ 21.48 (1C), 24.89 (3C), 55.86 (1C), 68.79 (3C), 127.41 (1C), 128.17 (2C), 128.84 (2C), 129.25 (1C), 130.15 (2C), 134.75 (2C), 141.14 (1C), 144.88 (1C). HRMS-m/z[M − Br]$^+$ calcd for $C_{20}H_{24}N^+$: 278.1909; found, 278.1910.

*5.1.2.18. 1-([1,1′-biphenyl]-4-ylmethyl)-3-hydroxyquinuclidin-1-ium bromide (**r**).* Following general procedure, after workup as described previously, compound **r** was isolated as a white solid. Yield: 63%, mp 260−262 °C. ^{1}H NMR (300 MHz, CD_3OD) δ 7.81 (d, *J* = 8.0 Hz, 2H), 7.69 (d, *J* = 7.7 Hz, 2H), 7.62 (d, *J* = 8.0 Hz, 2H), 7.50 (t, *J* = 7.5 Hz, 2H), 7.42 (t, *J* = 7.2 Hz, 1H), 4.33−4.72 (m, 2H), 4.04−4.34 (m, 1H), 3.76 (ddd, *J* = 11.6, 8.2, 2.7 Hz, 1H), 3.08−3.66 (m, 5H), 2.35 (m, 1H), 2.01−2.32 (m, 2H), 1.91 (ddd, *J* = 20.1, 9.7, 4.6 Hz, 2H). ^{13}C NMR (75 MHz, CD_3OD) δ 18.99 (1C), 22.59 (1C), 28.68 (1C), 54.74 (1C), 56.06 (1C), 64.64 (1C), 65.53 (1C) 68.69 (1C), 127.31 (1C), 128.25 (2C), 128.94 (2C), 129.34 (1C), 130.24 (2C), 134.81 (2C), 141.19 (1C), 145.06 (1C). HRMS-m/z[M − Br]$^+$ calcd for $C_{20}H_{24}NO^+$: 294.1858; found, 294.1860.

*5.1.2.19. 1-([1,1′-biphenyl]-4-ylmethyl)-7-chloro-4-(pyrrolidin-1-yl) quinolin-1-ium bromide (**s**).* Following general procedure, after workup as described previously, compound **s** was isolated as a white solid. Yield: 76%, mp 178−180 °C. ^{1}H NMR (300 MHz, CD_3OD) δ 1.66−2.42 (m, 4H), 2.99−3.60 (m, 4H), 5.83 (s, 2H), 6.93 (d, *J* = 7.7 Hz, 1H), 7.26−7.51 (m, 5H), 7.53−7.75 (m, 5H), 8.04 (d, *J* = 2.1 Hz, 1H), 8.57 (d, *J* = 7.7 Hz, 1H), 8.63 (d, *J* = 9.3 Hz. 1H). ^{13}C NMR (126 MHz, CD_3OD): δ 26.43 (2C), 54.97 (2C), 58.29 (1C), 103.87 (1C), 118.84 (1C), 119.29 (1C), 126.92 (1C), 127.95 (2C), 128.42 (2C), 128.75 (1C), 128.85 (2C), 129.95 (2C), 131.16 (1C), 134.73 (1C), 141.04 (1C), 141.37 (1C), 141.65 (1C), 142.95 (1C), 146.29 (1C), 157.11 (1C). HRMS-m/z[M − Br]+ calcd for $C_{26}H_{24}ClN_2^+$: 399.1628; found, 399.1631.

*5.1.2.20. 1-([1,1′-biphenyl]-4-ylmethyl)-4-(azepan-1-yl)-7-chloroquinolin-1-ium bromide (**t**).* Following general procedure, after workup as described previously, compound **t** was isolated as a white solid. Yield: 83%, mp 223−225 °C. ^{1}H NMR (300 MHz; CD_3OD) δ 1.77−1.63 (m, 4H), 2.10−2.06 (m, 4H), 4.07 (t, *J* = 5.6, 4H), 5.81 (s, 2H), 7.12 (d, *J* = 7.8, 1H), 7.44−7.31 (m, 5H), 7.66−7.58 (m, 5H), 8.06 (d, *J* = 2.0 Hz, 1H), 8.37 (d, *J* = 9.2, 1H), 8.55 (d, *J* = 7.8, 1H). ^{13}C NMR (75 MHz; CD_3OD) δ 26.86 (2C), 26.99 (2C), 53.84 (2C), 56.79 (1C), 102.37 (1C), 117.45 (1C), 117.56 (1C), 125.21 (1C), 126.52 (2C), 127.09 (2C), 127.32 (1C), 127.44 (2C), 128.51 (2C), 130.08 (1C), 133.18 (1C), 139.64 (1C), 139.93 (1C), 140.69 (1C), 141.57 (1C), 144.72 (1C), 159.30 (1C). HRMS-m/z[M − Br]$^+$ calcd for $C_{28}H_{28}N_2Cl^+$: 427.1941; found, 427.1933.

*5.1.2.21. 4-(azepan-1-yl)-1-([1,1′-biphenyl]-4-ylmethyl)-quinolin-1-ium bromide (**u**).* Following general procedure, after workup as described previously, compound **u** was isolated as a yellow solid. Yield: 72%, mp 223−225 °C· ^{1}H NMR (500 MHz, CD_3OD): δ 1.73 (m, 4H), 2.07 (m, 4H), 4.05 (m, 4H), 5.00 (s, 2H), 7.25 (d, *J* = 7.5 Hz, 1H), 7.35 (t, *J* = 7.4 Hz, 1H), 7.39 (d, *J* = 8.3 Hz, 2H), 7.43 (t, *J* = 7.6 Hz, 2H), 7.60 (d, *J* = 7.2 Hz, 2H), 7.67 (m, 3H), 8.12 (d, *J* = 1.9 Hz, 1H), 8.67 (d, *J* = 7.5 Hz, 1H), 8.21 (d, *J* = 9.1 Hz, 1H). ^{13}C NMR (126 MHz, CD_3OD): δ 23.35 (1C), 25.65 (2C), 53.36 (2C), 47.81 (1C), 57.11 (1C), 105.27 (1C), 117.99 (1C), 118.69 (1C), 126.30 (1C), 126.55 (2C), 127.18 (2C), 127.38 (1C), 127.50 (2C), 128.55 (2C), 129.35 (1C), 133.06 (1C), 139.93 (1C), 140.17 (1C), 140.57 (1C), 141.70 (1C), 145.95 (1C), 160.90 (1C). HRMS-m/z[M − Br]$^+$ calcd for $C_{28}H_{29}N_2Cl^+$: 413.1785; found, 413.1792.

*5.1.2.22. 1-([1,1′-biphenyl]-4-ylmethyl)-7-chloro-4-(methyl(phenyl) amino)quinolin-1-ium bromide (**v**).* Following general procedure, after workup as described previously, compound **v** was isolated as a yellow solid. Yield: 81%, mp 283−285 °C. **^{1}H NMR** (500 MHz, CD_3OD) δ 2.47 (s, 3H), 5.87 (s, 2H), 6.94 (d, *J* = 7.5 Hz, 1H), 7.48−7.37 (m, 10H), 7.60 (d, *J* = 7.2 Hz, 2H), 7.67 (d, *J* = 8.3 Hz, 2H), 7.84 (dd, *J* = 1.9, 9.1 Hz, 1H), 8.17 (d, *J* = 1.8 Hz, 1H), 8.63 (d, *J* = 8.5 Hz, 2H). ^{13}C NMR (125 MHz, CD_3OD) δ 19.75 (1C), 57.36 (1C), 100.59 (1C), 117.21 (1C), 118.31 (1C), 125.18 (2C), 125.63 (1C), 126.55 (2C), 127.00 (2C), 127.37 (1C), 127.51 (2C), 127.79 (1C), 128.54 (2C), 130.48 (2C), 133.11 (1C), 133.91 (1C), 138.58 (1C), 139.41 (1C), 139.93 (1C), 140.78 (1C), 141.69 (1C), 147.65 (1C), 156.00 (1C). HRMS-m/z[M − Br]$^+$ calcd for $C_{29}H_{24}N_2Cl^+$: 435.1628; found, 435.1626.

5.2. Biological assays and computational studies

5.2.1. Antiproliferative assays in cancer cells

Human cervix carcinoma (HeLa), and human colon adenocarcinoma (HT-29) cells were grown in DMEM medium (Gibco, Milan, Italy). B-acute lymphoblastic leukemia (RS4; 11) and T-acute lymphoblastic leukemia (CCRF-CEM) cells were grown in RPMI medium (Gibco, Milan, Italy). Both media were supplemented with 115 units/mL of penicillin G (Gibco, Milan, Italy), 115 μg/mL of streptomycin (Invitrogen, Milan, Italy) and 10% FCS (Invitrogen, Milan, Italy). Hela, Jurkat and HL-60 were purchased by DSMZ (Braunschweig, Germany), whereas HT-29 by ATCC. Cell lines were tested for mycoplasma contamination every 6 month by RT-PCR analysis. Stock solutions (10 mM) of the different compounds were obtained by dissolving them in DMSO. Individual wells of 96-well tissue-culture microtiter plates were inoculated with 100 μL of complete medium containing 8 × 10^3 cells. The plates were incubated at 37 °C in a humidified 5% CO_2 incubator for 18 h prior to the experiments. After medium removal, 100 μL of fresh medium containing the test compound at different concentrations was added to each well and incubated at 37 °C for 72 h. Cell viability was assayed by the (3-(4,5-dimethylthiazol-2-yl)-2,5-diphenyl tetrazolium bromide (MTT) test as previously described [31]. The GI_{50} was defined as the compound concentration required to inhibit cell proliferation by 50%, in comparison with cells treated with the maximum amount of DMSO (0.25%) and considered as 100% viability.

5.2.2. Cell cycle analysis

HeLa cells were treated with the test compounds for 24 h. Cells were harvested by centrifugation and fixed with 70% (v/v) cold

ethanol. Cells were lysed with 0.1% (v/v) Triton X-100 containing RNase A and stained with PI. A Beckman Coulter Cytomics FC500 instrument and MultiCycle for Windows software from Phoenix Flow Systems were used to analyze the cells.

5.2.3. Measurement of apoptosis by flow cytometry

The cells were treated with the test compounds and after different times stained with both PI, to stain DNA, and annexin V-fluorescein isothiocyanate, to stain membrane PS exposed on the cell surface, following the instructions of the manufacturer (Roche Diagnostics) of the Annexin-V-Fluos reagent.

5.2.4. Measurement of mitochondrial membrane potential

Mitochondrial potential was measured in HeLa cells by flow cytometry as previously described [20], using the fluorescent dye JC-1 (Molecular Probes).

5.2.5. Cloning and purification of CK

Details about cloning and purification of human CKα1 and CKβ have been previously reported [18].

5.3. Tryptophan fluorescence

All compounds were prepared in 100% DMSO. Before running the binding experiments, fluorescence property of the compounds was evaluated measuring the fluorescence signal at varying concentrations in a specific buffer (25 mM Tris, 150 mM NaCl, pH 7.5) containing an equivalent % of DMSO as the one used for the binding assay. The excitation wavelength was 280 nm while the emission was between 300 and 400 nm (typical emission range for protein tryptophan).

No fluorescence signal was detected for the compounds that could interfere with the binding assay.

The binding affinity constant (K_{ds}) of the compounds against human CKα1 and CKβ, were measured by monitoring the quenching of tryptophan fluorescence. All experiments were carried out in a Cary Eclipse spectrofluorometer (Varian) at 25 °C with the enzymes at 1 mM, and concentrations of compounds varying from 0.1 to 10 mM for *Hs*CKα1 and 0.5–200 mM for *Hs*CKβ in 25 mM Tris, 150 mM NaCl, pH 7.5. Fluorescence emission spectra were recorded in the 300–400 nm range with an excitation wavelength of 280 nm, with slit width of 5 nm. Controls were determined by incubating the enzymes with equivalent amounts of DMSO. As indicated previously, data analysis was performed in Prism 6 (GraphPad software) [32] considering a model with a single binding site (Equation (1)), where F0 is the intrinsic fluorescence of the enzyme in the absence of quencher (Q), F1 is the observed fluorescence at a given quencher concentration, fa is the fractional degree of fluorescence, and K_d is the dissociation constant.

$$1 - \frac{F1}{F0} = fa \times \frac{[Q]}{Kd + [Q]} \quad (1)$$

5.3.1. Protein crystallography

Human ChoKα1 at 20 mg/mL was preincubated at room temperature with 25 mM hit b and 30 mM hit o in buffer 25 mM Tris/HCl, 150 mM NaCl pH 7.5 (DMSO is at 5% final concentration in the mix). The sitting-drop vapor diffusion [33] method was used to produce crystals by mixing 0.5 mL of the protein solution and an equal volume of mother liquor. Crystals of the human ChoKα1-compound b complex appeared in 18% polyethylene glycol (PEG) 3350 and 0.1 M potassium chloride, whereas crystals of the human ChoKα1-compound o complex appeared in 20% PEG 3350 and 0.2 M magensium nitrate. Both orthorhombic (space group $P2_12_12_1$ for crystals of the human ChoKα1-compound b complex) and tetragonal crystals (space group $P4_32_12$ for crystals of the human ChoKα1-compound o complex) grew within 3–14 days. The crystals used in this study were cryoprotected in mother liquor solutions containing 20% ethylenglycol and frozen in a nitrogen gas stream cooled to 100 K. Diffraction data of the binary complexes were collected at beamline I04–1 (Diamond, Oxford; experiment MX8035-11) and XALOC (ALBA, Barcelona). The data was processed and scaled using the XDS package [34] and CCP4 software [35]: relevant statistics are given in Table 4.

5.3.2. Structure determination and refinement

The structure of the binary complex was solved by molecular replacement using PDB entry 3G15 as a template. Initial phases were further improved by cycles of manual model building in Coot [36] and refinement with REFMAC5 [37]. The final model was validated with PROCHECK [38], model statistics are given in Table 4. Coordinates and structure factors have been deposited in the Worldwide Protein Data Bank.

5.3.3. Determination of human choline kinase α1 activity

The effect of the different inhibitors on human CK was assayed in CKα1 purified as previously described [21]. In each experiment DMSO-assays were consistently run in parallel as a control. DMSO in no case exceeded a concentration of 0.1% in order to avoid unspecific CK inhibition. CK activity was assayed by measuring the rate of incorporation of ^{14}C from [methyl-^{14}C]choline (PerkinElmer, Massachusetts, USA) into PC both in the presence or absence of different inhibitor concentrations. Briefly, the final reaction mixture contained 100 mM Tris (pH 8.5), 10 mM $MgCl_2$, and 10 mM ATP, and 20 ng of purified CKα1. After the samples were preincubated at 37 °C for 5 min, the reaction was initiated with 1 mM [methyl-^{14}C] choline (4500 dpm/nmol) and incubated at 37 °C for 10 min, the final volume being 55 μL. The assay was stopped by immersing the reaction tubes in boiling water for 3 min. Aliquots of the reaction mixture were applied to the origin of Silica Gel plates (Analtech, Newark, USA) in the presence of PC (0.1 mg) and choline (0.1 mg) as carriers. The chromatography was developed in methanol/0.6% NaCl/28% NH_4OH in water (50:50:5, v/v/v) as solvent. PC was visualized under exposure to iodine vapor, and the corresponding spot was scraped and transferred to scintillation vials for measurement of radioactivity by a Beckman 6000-TA (Madrid, Spain) liquid-scintillation counter. At least three experiments were performed in all assays. The 50% inhibitory concentrations (IC_{50} values) were determined from the % activity of the enzymes at different concentrations of synthetic inhibitors by using a sigmoidal dose-response curve (the ED_{50}plus v1.0 software).

5.3.4. Docking studies

Details about computational studies have been previously reported [22].

5.3.5. Choline uptake assay

Choline uptake was determined as previously reported [39]. Briefly, HepG2and HT-29 cells (200,000 cells/well) were incubated for 10 min at 37 °C either in a medium containing different concentrations of CKα1 inhibitors or with no supplement as controls. The medium was then removed and the cells immediately exposed to a medium containing [methyl-^{14}C]choline (16 μM, 31 Ci/mol) for 5 min at 37 °C. The incorporation of choline was stopped by medium aspiration followed by two washes with ice-cold PBS containing 580 μM choline. The cells were solubilized in NaOH 0.1 N and an aliquot used to determine the total amount of radiolabel taken up by the cells.

5.3.6. Statistical analysis

Graphs and statistical analyses were performed using GraphPad Prism software (GraphPad, La Jolla, CA, USA). All data in graphs represented the mean of at least three independent experiments ± SEM. Statistical significance was determined using Student's t-test or ANOVA (one- or two-way) depending on the type of data. Asterisks indicate a significant difference between the treated and the control group, unless otherwise specified. *$p < 0.05$, **$p < 0.01$, ***$p < 0.001$, ****$p < 0.0001$.

Declaration of competing interest

The authors declare that they have no known competing financial interests or personal relationships that could have appeared to influence the work reported in this paper.

Acknowledgments

The authors are grateful to the Centro de Servicios de Informática and the Centro de Instrumentación Científica of the University of Granada (Spain) for the use of their computers and scientific software. We acknowledge to "PID2019-109294RB-I00. Convocatoria 2019 Proyectos de I + D + i - RTI Tipo B. Ministerio de Innovación y Ciencia"for its financial support. R.H.-G. acknowledges ALBA Light Source (Barcelona, Spain) synchrotron beamline XALOC and the Diamond Light Source (Oxford, UK) synchrotron beamline I04-1 (experiment number MX8035-11). He also acknowledges ARAID, MEC (CTQ2013-44367-C2-2-P, BFU2016-75633-P and PID2019-105451 GB-I00) and Gobierno de Aragón (E34_R17 and LMP58_18) with FEDER (2014–2020) funds for 'Building Europe from Aragón' for financial support. The research leading to these results has also received funding from FP7 442 (2007–2013) under BioStruct-X (grant agreement no. 283570 and BIOSTRUCTX_5186).

Appendix A. Supplementary data

Supplementary data to this article can be found online at https://doi.org/10.1016/j.ejmech.2020.112797.

References

[1] R. Straussman, T. Morikawa, K. Shee, M. Barzily-Rokni, Z.R. Qian, J. Du, A. Davis, M.M. Mongare, J. Gould, D.T. Frederick, Z.A. Cooper, P.B. Chapman, D.B. Solit, A. Ribas, R.S. Lo, K.T. Flaherty, S. Ogino, J.A. Wargo, T.R. Golub, Tumour micro-environment elicits innate resistance to RAF inhibitors through HGF secretion, Nature 487 (2012) 500–504.
[2] B. Kalyanaraman, G. Cheng, M. Hardy, O. Ouari, M. Lopez, J. Joseph, J. Zielonka, M.B. Dwinell, A review of the basics of mitochondrial bioenergetics, metabolism, and related signaling pathways in cancer cells: therapeutic targeting of tumor mitochondria with lipophilic cationic compounds, Redox Biol 14 (2018) 318–327.
[3] G. Luo, N. Liu, Int. J. Mol. Med. 28 (2018) 1–10.
[4] K. Glunde, M.F. Penet, L. Jiang, M.A. Jacobs, Z.M. Bhujwalla, Choline metabolism-based molecular diagnosis of cancer: an update, Expert Rev. Mol. Diagn 15 (2015) 735–747.
[5] T. Shah, B. Krishnamachary, F. Wildes, J.P. Wijnen, K. Glunde, Z.M. Bhujwalla, Molecular causes of elevated phosphoethanolamine in breast and pancreatic cancer cells, NMR Biomed. 31 (2018), e3936.
[6] F. Gibellini, T.K. Smith, The Kennedy Pathway–De Novo Synthesis of Phosphatidylethanolamine and Phosphatidylcholine *IUBMB Life*, vol. 62, 2010, pp. 414–428.
[7] M. Agassandian, R.K. Mallampalli, Surfactant phospholipid metabolism, Biochim. Biophys. Acta 1831 (2013) 612–625.
[8] M. Cheng, Z.M. Bhujwalla, K. Glunde, Targeting phospholipid metabolism in cancer, Front Oncol 6 (2016) 266–282.
[9] S.P. Arlauckas, A.V. Popov, E.J. Delikatny, Choline kinase alpha-Putting the ChoK-hold on tumor metabolism, Prog. Lipid Res. 63 (2016) 28–40.
[10] R.B. Cornell, N.D. Ridgway, CTP:phosphocholine cytidylyltransferase: function, regulation, and structure of an amphitropic enzyme required for membrane biogenesis, Prog. Lipid Res. 59 (2015) 147–171.
[11] A. Rodríguez-González, A. Ramírez de Molina, F. Fernández, J.C. Lacal, Choline kinase inhibition induces the increase in ceramides resulting in a highly specific and selective cytotoxic antitumoral strategy as a potential mechanism of action, Oncogene 23 (2004) 8247–8259.
[12] J. Xiong, J. Bian, L. Wang, J.Y. Zhou, Y. Wang, Y. Zhao, L. L Wu, J.J. Hu, B. Li, S. J Chen, C. Yan, W. L Zhao, Dysregulated choline metabolism in T-cell lymphoma: role of choline kinase-α and therapeutic targeting, Blood Canc. J. 5 (2015) 287.
[13] S. Schiaffino-Ortega, E. Baglioni, E. Mariotto, R. Bortolozzi, L. Serrán-Aguilera, P. Ríos-Marco, M.P. Carrasco-Jimenez, M.A. Gallo, R. Hurtado-Guerrero, C. Marco, G. Basso G. Viola A. Entrena, L.C. López-Cara, Design, synthesis, crystallization and biological evaluation of new symmetrical biscationic compounds as selective inhibitors of human Choline Kinase α1 (ChoKα1), Sci. Rep. 6 (2016) 23793.
[14] A. Sola-Leyva, L.C. López-Cara, P. Ríos-Marco, A. Ríos, C. Marco, M.P. Carrasco-Jiménez, Choline kinase inhibitors EB-3D and EB-3P interferes with lipid homeostasis in HepG2 cells, Sci. Rep. 9 (2019) 5109.
[15] E. Mariotto, R. Bortolozzi, I. Volpin, D. Carta, V. Serafin, B. Accordi, Navarro P. Luque, L.C. Lopez Cara, G. Basso, G. Viola, EB-3D a novel choline kinase inhibitor induces deregulation of the AMPK-mTOR pathway and apoptosis in leukemia T-cells, Biochem. Pharmacol. 155 (2018) 213–223.
[16] E. Mariotto, G. Viola, R. Ronca, Z.M. Bhujwalla, B. Accordi, V. Serafin, L. Persano, L.C. Lopez Cara, R. Bortolozzi, The novel choline kinase alpha inhibitor EB-3D induces cellular senescence reduce tumor growth and metatastic dissemination in breast cancer *Cancers* 10 (2018) 391.
[17] M. Sahún-Roncero, B. Rubio-Ruiz, G. Saladino, A. Conejo-García, A. Espinosa, A. Velázquez-Campoy, F.L. Gervasio, A. Entrena, R. Hurtado-Guerrero, The mechanism of allosteric coupling in choline kinase α1 revealed by the action of a rationally designed inhibitor, Angew. Chem., Int. Ed. Engl. 52 (2013) 4582–4586.
[18] M. Sahún -Roncero, B. Rubio-Ruíz, A. Conejo-García, A. Velazquez-Campoy, A. Entrena, R. Hurtado-Guerrero, Determination of potential scaffolds for human choline kinase α1 by chemical deconvolution studies, Chembiochem 14 (2013) 1291–1295.
[19] B. Rubio-Ruiz, A. Figuerola-Conchas, J. Ramos-Torrecillas, F. Capitan-Canadas, P. Ríos-Marco, M.P. Carrasco, M.A. Gallo, A. Espinosa, C. Marco, C. Ruiz, A. Entrena, R. Hurtado-Guerrero, A. Conejo-García, Discovery of a new binding site on human choline kinase α1: design, synthesis, crystallographic studies, and biological evaluation of asymmetrical bispyridinium derivatives, J. Med. Chem. 57 (2014) 507–515.
[20] F. Fermin Castro-Navas, S. Schiaffino-Ortega, M.P. Carrasco-Jimenez, P. Ríos-Marco, C. Marco, A. Espinosa, M.A. Gallo, G. Basso, R. Bortolozzi, G. Viola, A. Entrena, L.C. López-Cara, New more polar symmetrical bipyridinic compounds: new strategy for the inhibition of choline kinase α1, *Future Med. Chem* . 4 (2015) 417–436.
[21] G. Rubbini, Ana B. Buades-Martín, María Kimatrai-Salvador, Antonio Entrena, M.Á. Gallo-Mezo, P. Ríos-Marco, C. Marco, E. Mattiuzzo, R. Bortolozzi, E. Mariotto, F.A. Greco, A. Macchiarulo, M.P. Carrasco-Jiménez, G. Viola, L.C. López-Cara, Lead optimization-hit expansion of new asymmetrical pyridinium/quinolinium compounds as ChoKα1 inhibitors, Future Med. Chem. 10 (2018) 1769–1786.
[22] L. Serrán-Aguilera, R. Nuti, L.C. López-Cara, M.Á. Gallo Mezo, A. Macchiarulo, A. Entrena, R. Hurtado-Guerrero, Pharmacophore-based virtual screening to discover new active compounds for human choline kinase α1, Molecular Informatics 34 (2015) 458–466.
[23] L. Serran-Aguilera, R. Nuti, L.C. López-Cara, P. Ríos-Marco, M. P Carrasco, C. Marco, A. Entrena, A. Macchiarulo, R. Hurtado-Guerrero, Choline kinase active site provides features for designing versatile inhibitors, Curr. Top. Med. Chem. 14 (2014) 2684–2693.
[24] S.G. Zech, A. Kohlmann, T. Zhou, F. Li, R.M. Squillace, L.E. Parillon, M.T. Greenfield, D.P. Miller, J. QiR, M. Thomas, Y. Wang, Y. Xu, J.J. Miret, W.C. Shakespeare, X. Zhu, D.C. Dalgarno, Novel small molecule inhibitors of choline kinase identified by fragment-based drug discovery, J. Med. Chem. 59 (2016) 671–686.
[25] S. Schiaffino-Ortega, L.C. López-Cara, P. Ríos-Marco, M.P. Carrasco-Jimenez, M. A Gallo, A. Espinosa, Carmen Marco, Antonio Entrena, Bioorg. Med. Chem. 21 (2013) 7146–7154.
[26] J. Gruber, W.C. See Too, M.T. Wong, A. Lavie, T. McSorley, M. Konrad, Balance of human choline kinase isoforms is critical for cell cycle regulation: implications for the development of choline kinase-targeted cancer therapy, FEBS J. 279 (2012) 1915–1928.
[27] C.S. Hudson, R.M. Knegtel, K. Brown, P.A. Charlton, J.R. Pollard, Kinetic and mechanistic characterisation of choline kinase-alpha, Biochim. Biophys. Acta 1834 (2013) 1107–1116.
[28] V. Michel, Z. Yuan, S. Ramsubir, M. Bakovic, Choline transport for phospholipid synthesis, Exp. Biol. Med. 231 (2006) 490–504.
[29] T. Hara, A. Bansal, T.R. DeGrado, Choline transporter as a novel target for molecular imaging of cancer, Mol. Imag. 5 (2006) 498–509.
[30] M. Inazua, T. Yamada, N. Kubota, T. Yamanaka, Functional expression of choline transporter-like protein 1 (CTL1) in small cell lung carcinoma cells: a target molecule for lung cancer therapy, Pharmacol. Res. 76 (2013) 119–131.
[31] F.J. Bock Tait SWG, Mitochondria as multifaceted regulators of cell death, Nat. Rev. Mol. Cell Biol. 21 (2020) 85–100.
[32] www.graphpad.com.
[33] H. Adachi, K. Takano, M. Morikawa, S. Kanaya, M. Yoshimura, Y. Mori, T. Sasaki, Acta Crystallogr. D Biol. Crystallogr. 59 (2003) 194–196.
[34] W. Kabsch, Acta Crystallogr. D Biol. Crystallogr. 66 (2010) 125–132.

[35] A.J. McCoy, R.W. Grosse-Kunstleve, P.D. Adams, M.D. Winn, L.C. Storoni, R.J. Read, J. Appl. Crystallogr. 40 (2007) 658–674.
[36] P. Emsley, K. Cowtan, Acta Crystallogr. D Biol. Crystallogr. 60 (2004) 2126–2132.
[37] A.A. Vagin, R.A. Steiner, A.A. Lebedev, L. Potterton, S. McNicholas, F. Long, G.N. Murshudov, Acta Crystallogr. D Biol. Crystallogr. 60 (2004) 2184–2195.
[38] a) R.A. Laskowski, J.A. Rullmannn, M.W. MacArthur, R. Kaptein, J.M. Thornton, J. Biomol. NMR 8 (1996) 477–486;
b) , in: http://www.ebi.ac.uk/thornton-srv/software/PROCHECK/index. html.
[39] J.M. Jiménez-López, M.P. Carrasco, J.L. Segovia, C. Marco, Hexadecylphosphocholine inhibits phosphatidylcholine biosynthesis and the proliferation of HepG2 cells, Eur. J. Biochem. 269 (2002) 4649–4655.